Structural basis of death domain signaling in the p75 neurotrophin receptor

Zhi Lin[1,2], Jason Y. Tann[1,2], Eddy T. H. Goh[1,2], Claire Kelly[3], Kim Buay Lim[1,2], Jianfang Gao[1,2] and Carlos F. Ibáñez [1,2,3*]

[1] Department of Physiology, National University of Singapore, Singapore 117597, Singapore

[2] Life Sciences Institute, National University of Singapore, Singapore 117456, Singapore

[3] Department of Neuroscience, Karolinska Institute, Stockholm S-17177, Sweden

[*] Corresponding author: phscfi@nus.edu.sg; Tel: +65 6516 5889; Fax: +65 6777 3271

Abbreviations: CARD, caspase recruitment domain; DD, death domain; EGFP, Enhanced Green Fluorescent Protein; FRET, Fluorescence resonance energy transfer; NGF, nerve growth factor; $p75^{NTR}$, p75 neurotrophin receptor; RhoGDI, Rho guanine nucleotide dissociation inhibitor; RIP2, Receptor Interacting Protein kinase 2; RMSD, root mean square deviation; TM, transmembrane domain; TNFRSF, tumor necrosis factor receptor superfamily.

Keywords: CARD, NMR, p75ntr, solution structure, RhoGDI, RhoA, RIP2

Running title: Structural basis of death domain signaling in $p75^{NTR}$

Abstract

Death domains (DDs) mediate assembly of oligomeric complexes for activation of downstream signaling pathways through incompletely understood mechanisms. Here we report structures of complexes formed by the DD of p75 neurotrophin receptor ($p75^{NTR}$) with RhoGDI, for activation of the RhoA pathway, with caspase recruitment domain (CARD) of RIP2 kinase, for activation of the NF-kB pathway, and with itself, revealing how DD dimerization controls access of intracellular effectors to the receptor. RIP2 CARD and RhoGDI bind to $p75^{NTR}$ DD at partially overlapping epitopes with over 100-fold difference in affinity, revealing the mechanism by which RIP2 recruitment displaces RhoGDI upon ligand binding. The $p75^{NTR}$ DD forms non-covalent, low-affinity symmetric dimers in solution. The dimer interface overlaps with RIP2 CARD but not RhoGDI binding sites, supporting a model of receptor activation triggered by separation of DDs. These structures reveal how competitive protein-protein interactions orchestrate the hierarchical activation of downstream pathways in non-catalytic receptors.

Introduction

The death domain (DD) is a globular protein module of 80 to 90 amino acid residues with a characteristic 6-helix bundle fold (Feinstein et al., 1995; Ferrao and Wu, 2012). DDs are present in a variety of proteins, including several members of the tumor necrosis factor receptor superfamily (TNFRSF) and a range of intracellular signaling components, such as caspases and kinases. The DD family includes four subfamilies of structurally related domains, including the canonical DD, the death effector domain (DED), the caspase recruitment domain (CARD) and the pyrin domain (PYD). DD-containing proteins play central roles in apoptotic and inflammatory signaling through the formation of oligomeric protein complexes, and several disease-causing mutations have been mapped to DD interfaces (Park et al., 2007a). All DD complexes described so far involve homotypic interactions between DDs of the same subfamily (e.g. DD with DD, CARD with CARD, etc.). All known DD interactions belong to one of three types (I to III), each mediated by conserved asymmetric interfaces in the interacting DDs (Park, 2011; Park et al., 2007b; Weber and Vincenz, 2001). Heterotypic complexes between DDs from different subfamilies have not yet been described and, aside from a few structures of DDs bound to small polypeptides, no complexes of DDs with proteins outside the DD superfamily have been reported. Thus, type I, II and III interactions between DDs are thought to represent the predominant mechanism of oligomerization and complex formation for DD-containing proteins.

The cytoplasmic domain of the p75 neurotrophin receptor ($p75^{NTR}$, also known as NGFR and TNFRSF16) contains a C-terminal DD connected to the transmembrane (TM) domain by a 60 residue-long linker region (Liepinsh, 1997). $p75^{NTR}$ is a receptor for members of the neurotrophin family, such as nerve growth factor (NGF) and brain-derived neurotrophic factor (BDNF) (Dechant and Barde, 2002; Roux and Barker, 2002). In addition to the neurotrophins, a number of other extracellular ligands can also engage or signal through $p75^{NTR}$, including the beta-amyloid peptide (Knowles et al., 2009; Perini et al., 2002), the rabies virus glycoprotein (Tuffereau et al., 1998), and

various myelin-derived polypeptides (Wang et al., 2002; Wong et al., 2002). $p75^{NTR}$ may function alone or in conjunction with other transmembrane proteins to allow ligand binding and intracellular signaling. These proteins include members of the Trk family of receptor tyrosine kinases, members of the Vps10p family of sorting receptors, such as Sortilin, and the Nogo receptor, which promotes binding to myelin-derived ligands (Underwood and Coulson, 2008). $p75^{NTR}$ can engage different intracellular pathways, of which the best characterized are the RhoA pathway, which regulates axon growth, collapse and degeneration (Park et al., 2010; Yamashita et al., 1999; Yamashita and Tohyama, 2003), the NF-kB pathway, which contributes to cell survival (Carter et al., 1996; Khursigara et al., 2001; Vicario et al., 2015), and the c-Jun kinase (JNK) or caspase pathway, which mediates apoptotic cell death (Friedman, 2000; Yoon et al., 1998). $p75^{NTR}$ signaling through any of those three pathways requires a functional DD (Charalampopoulos et al., 2012). Expression of $p75^{NTR}$ increases in a number of neurodegenerative diseases and upon injury or stress conditions, where it contributes to neuronal and glial cell damage, axonal degeneration and synaptic dysfunction (Ibanez and Simi, 2012). Inhibition of $p75^{NTR}$ signaling has emerged as an attractive strategy for limiting neural damage in neurodegeneration and nerve injury.

The mechanism of activation of $p75^{NTR}$ in response to neurotrophins involves a conformational rearrangement of disulphide-linked receptor dimers resulting in the separation of intracellular DDs (Vilar et al., 2009). Fluorescence resonance energy transfer (FRET) experiments have shown that the two DDs in the $p75^{NTR}$ dimer are in close proximity to each other (high FRET state) and that NGF binding induces a decrease in FRET signal (Vilar et al., 2009). Disruption of this conformational change through mutation of a conserved cysteine residue in the TM domain prevents $p75^{NTR}$ signaling in response to neurotrophins (Vilar et al., 2009). $p75^{NTR}$ lacks an associated catalytic activity. Similar to other members of the TNFRSF, signaling by $p75^{NTR}$ proceeds via ligand-induced recruitment and release of cytoplasmic effectors to and from its intracellular domain. Ligand-induced separation of $p75^{NTR}$ DDs may allow the recruitment of intracellular components for downstream signal propagation. Although a

variety of intracellular proteins have been reported to interact with $p75^{NTR}$, the molecular mechanisms by which the receptor engages different signaling pathways remain unclear. To begin addressing these questions, our laboratory performed a comprehensive structure-function study of the $p75^{NTR}$ DD that resulted in the identification of three sets of solvent-exposed residues that are critical for $p75^{NTR}$'s ability to engage the RhoA, NF-kB and JNK/cell death pathways, respectively (Charalampopoulos et al., 2012). Receptor mutants that are selectively deficient in one pathway but not others were generated, demonstrating that different signaling outputs can be genetically separated in $p75^{NTR}$. Understanding how such interfaces relate to each other and to the mechanism of receptor activation has remained an important challenge.

In this study, we have undertaken a structural biology approach to elucidate the molecular mechanisms underlying downstream signaling mediated by the DD in $p75^{NTR}$. We have determined the solution structures of the $p75^{NTR}$ DD in complex with RhoGDI (Rho guanine nucleotide dissociation inhibitor), which links the receptor to the RhoA pathway (Yamashita et al., 1999; Yamashita and Tohyama, 2003), or with the CARD domain of RIP2 kinase, which is necessary for $p75^{NTR}$ coupling to the NF-kB pathway (Charalampopoulos et al., 2012; Khursigara et al., 2001). We have also solved the solution structure of the $p75^{NTR}$ DD homodimer, revealing the DD surface that is occluded prior to neurotrphin-medaited receptor activation. These structures uncover novel heterotypic DD interactions, not previously seen in other DD-containing complexes, and reveal the molecular mechanisms underlying the early stages of $p75^{NTR}$ activation and downstream signaling.

Results

Solution structure of the complex between the p75^{NTR} DD and RhoGDI

RhoGDI interacts constitutively with the DD of unliganded p75^{NTR}, linking the receptor to the RhoA pathway (Yamashita and Tohyama, 2003). Neurotrophin binding induces the release of RhoGDI from p75^{NTR} and decreases RhoA activity (Gehler et al., 2004; Yamashita et al., 1999; Yamashita and Tohyama, 2003). Using biochemical and cell-based assays, we have previously identified solvent-exposed residues in the p75^{NTR} DD that are critical for its interaction with RhoGDI and RhoA activation, including residues in helices H1 and H6 (Charalampopoulos et al., 2012). In order to obtain a molecular understanding of this interaction, we determined the solution structure of the human p75^{NTR} DD:RhoGDI complex by multidimensional nuclear magnetic resonance (NMR) spectroscopy (Figure 1—figure supplement 1 and Table 1). We note that, unless otherwise indicated, all amino acid residue numbering in this study corresponds to the human forms of the respective proteins. Human and rat p75^{NTR} DD share more than 90% sequence identity —including all functionally-relevant residues— and an essentially identical three-dimensional structure with an overall RMSD of 1.7Å ((Liepinsh, 1997) and this study). The ensemble of the ten lowest-energy conformers of the DD:RhoGDI complex and a representative structure are depicted in Figures 1A and 1B. p75^{NTR} DD in the complex consists of one 3_{10}-helix followed by six α-helices and its global fold is very similar to that of our previously described structure of rat p75^{NTR} DD (Liepinsh, 1997). In the complex, the C-terminal domain of RhoGDI primarily displays an immunoglobulin-like fold similar to previously described structures of this protein (Longenecker et al., 1999). Residues Glu^{40} to Gly^{57} in the RhoGDI N-terminal domain fold into a long helix which is not involved in p75^{NTR} DD binding and remains flexible in the complex (Figure 1A). Removal of this N-terminal domain did not affect RhoGDI binding to p75^{NTR} DD (Figure 1—figure supplement 2). Inspection of the interface in the complex showed that it is mainly formed by α-helices H1 and H6 of the p75^{NTR} DD and β-strands S2, S3, S9 and α-helix H2 of RhoGDI, forming a small

hydrophobic core surrounded by polar residues (Figure 1C). Charged residues play an important role in the binding interface and salt high-concentration (i.e. greater than 200mM NaCl) can almost completely disrupt $p75^{NTR}$ DD:RhoGDI interaction *in vitro* (Figure 1—figure supplement 1C). It is gratifying to note that all functional DD determinants that we have previously identified by site-directed mutagenesis clustered at the DD:RhoGDI interface of the complex structure (labeled red in Figures 1C and 1D). The structure of the DD:RhoGDI complex offered an opportunity to address the functional importance of a larger set of residues in the $p75^{NTR}$ DD as well as in RhoGDI. Co-immunoprecipitation experiments were performed in cells transfected with constructs of full-length $p75^{NTR}$ and RhoGDI carrying different point mutations in selected residues. Alanine substitution of individual amino acid residues likely uncovers only those side chains making the most critical contribution to the binding interface. In the $p75^{NTR}$ DD, substitution of either Asp^{412}, Lys^{343} or Glu^{420} was found to significantly diminish interaction with RhoGDI (Figure 1D). In RhoGDI, substitution of Lys^{99} or Lys^{199} abolished its interaction with $p75^{NTR}$ (Figure 1E). In agreement with this, the structure of the complex shows that these two positively charged side chains make charge interactions with Glu^{420} and Asp^{412}, respectively, in the $p75^{NTR}$ DD (Figure 1C).

Analysis of the $p75^{NTR}$ DD:RhoGDI complex and a previously described crystal structure of the RhoGDI:RhoA(GDP) complex (Longenecker et al., 1999) indicated that $p75^{NTR}$ DD and RhoA interact with different surfaces in RhoGDI, located at opposite sides of the molecule. The two distant binding sites on RhoGDI suggested that a heterotrimer complex $p75^{NTR}$ DD:RhoGDI:RhoA may be structurally feasible. We investigated this by performing HADDOCK calculations (Dominguez et al., 2003) using our solution structure of $p75^{NTR}$ DD from its complex with RhoGDI and the crystal structure of the RhoGDI:RhoA(GDP) complex. Multiple refinements converged to a mean backbone root mean square deviation (RMSD) of 0.64±0.05Å (Figures 2A, 2B and Table 2). Ramachandran plot analysis of the docking model indicated that the trimer structure, including the two intermolecular interfaces, still occupies the energetically preferred conformation. In the tripartite complex, the N-terminal domain of

RhoGDI folded into two helices and bound to RhoA(GDP), similar to its conformation in the RhoGDI:RhoA(GDP) complex (Longenecker et al., 1999). The DD binding site on RhoGDI remained nearly identical to that in the DD:RhoGDI complex. This analysis shows that interaction of the three proteins can indeed occur simultaneously and explains previous biochemical studies showing that RhoA can be co-immunoprecipitated with $p75^{NTR}$ in the presence of RhoGDI (Yamashita et al., 1999). Using the purified proteins, we determined the binding affinity of the RhoGDI:RhoA complex by surface plasmon resonance (SPR). Titration of RhoGDI onto immobilized RhoA, yielded a binding Kd of 0.14±0.01 μM, which is in agreement with previous measurements (Tnimov et al., 2012) (Figure 2C). Interestingly, when RhoGDI was precomplexed with purified $p75^{NTR}$ DD, the Kd was 2.2±0.11 μM (Figure 2D), indicating that binding to the $p75^{NTR}$ DD decreases the affinity of the RhoGDI:RhoA interaction by about 15-fold. We note that, in the absence of RhoGDI, no binding between $p75^{NTR}$ DD and RhoA could be detected in these experiments (Figure 2E). These results suggest that RhoGDI binding to the $p75^{NTR}$ DD weakens its interaction with RhoA, a step which may facilitate RhoA activation.

Solution structure of the complex between the $p75^{NTR}$ DD and RIP2 CARD

NGF binding to $p75^{NTR}$ elicits the recruitment of RIP2 kinase to the receptor. Recruitment of RIP2 is required for regulation of the NF-kB pathway by $p75^{NTR}$. Previous biochemical studies established that the interaction between $p75^{NTR}$ and RIP2 is mediated by their DD and CARD domains, respectively (Khursigara et al., 2001). The RIP2 CARD consists of 107 amino acids and is located in the C-terminal of the protein. It connects to the N-terminal kinase domain via a linker of 120 amino acids. We determined the NMR structure of human RIP2 CARD in monomeric form (Figures 3A, 3B and Table 1). The solution structure of RIP2 CARD comprises an arrangement of six α-helices followed by one short 3_{10}-helix, all tightly packed around a hydrophobic core. A C-terminal tail of 17 amino acids (Leu^{524}-Met^{540}) follows the CARD and is unstructured and flexible in solution. A unique segment (Gln^{518}-Ile^{523}) between

the C-terminal tail and the 3_{10}-helix contains two structural disruptor residues (i.e. Pro^{519} and Pro^{520}, Figure 3B) and lacked secondary structure, but its orientation was well-defined in the NMR structure. A number of hydrophobic residues (e.g. Ile^{523}, Figure 3B) in this segment closely interact with the first and the last α-helices in the RIP2 CARD. Structural comparison using the DALI server (Holm and Rosenström, 2010) showed that the most similar structure to RIP2 CARD was the CARD of nucleotide-binding oligomerization domain-containing protein 1 (NOD1), with a Z-score between 9 and 11. NOD1 and RIP2 have been shown to interact with each other through their CARDs to propagate immune signaling (Mayle et al., 2014). The two CARDs share similar structural features, including a similar arrangement of all but the last of the α-helices, which displays different local secondary structures in the two proteins (Figure 3—figure supplement 1A). Despite their folding similarities, the two CARDs exhibit significantly different surface characteristics. Particularly, RIP2 CARD has many more charged residues on its surface than its NOD1 counterpart (Figure 3—figure supplement 1B and C). Different electrostatic surfaces will confer different interaction specificities, a common feature among members of the DD superfamily, including the CARD subfamily.

In order to obtain a molecular understanding of the $p75^{NTR}$ DD:RIP2 CARD interaction, we determined the NMR structure of the complex. Figures 3C and 3D present the three-dimensional solution structure of this complex obtained from the NMR experimental restraints (Table 1 and Figure 3—figure supplement 2). The core helical structure of the $p75^{NTR}$ DD in the $p75^{NTR}$ DD:RIP2 CARD complex was similar to that in the $p75^{NTR}$ DD:RhoGDI complex, with a pairwise RMSD of ~1.9 Å (Figure 3—figure supplement 3A). The orientation of α-helices H3 and H6 changed by approximately 7-8°. Similarly, pairwise RMSD between RIP2 CARD in monomeric form and in complex with the $p75^{NTR}$ DD was ~1.5 Å (Figure 3—figure supplement 3B). The main interface in the core structure of the $p75^{NTR}$ DD:RIP2 CARD complex involved α-helices H2, H3, H5, H6 and H5-H6 loop of $p75^{NTR}$ DD and α-helices H1, H3-H4 and H5-H6 loops of RIP2 CARD (Figures 3E and 3F). Both electrostatic and hydrophobic interactions

contribute to the p75^{NTR} DD:RIP2 CARD interface. Interestingly, the C-terminal tail of RIP2 CARD was better defined in its complex with the p75^{NTR} DD compared to its monomeric form, although the last six amino acids still remained flexible. The C-terminal tail bound to α-helices H1, H5 and H6 of p75^{NTR} DD, through both hydrophobic and charged interactions (Figure 3D and Figure 3—figure supplement 3B). In our previous site-directed mutagenesis studies of the p75^{NTR} DD, we had identified residues in helices H2 (Asp^{357}, His^{361} and Glu^{365}), H3 (Gln^{369} and Glu^{371}), H5 (Asp^{399}) and H6 (Asp^{412} and Glu^{415}) as being critical for its interaction with RIP2 (Charalampopoulos et al., 2012). We were pleased to note that all these residues mapped to the DD:CARD binding interface defined in our NMR structure of the complex (labeled red in Figures 3E and 3F). The NMR structure of the DD:CARD complex offered an opportunity to address the functional importance of residues in the RIP2 CARD. Co-immunoprecipitation experiments were performed in cells transfected with constructs of full-length p75^{NTR} and RIP2, the latter carrying different point mutations in selected residues of the CARD. We found that individual substitution of interface residues Gln^{437}, Asp^{467}, Lys^{471}, Ile^{496}, Glu^{500} or Arg^{528}, significantly diminished RIP2 interaction with p75^{NTR} (Figure 3G).

Differential binding of RhoGDI and RIP2 CARD to the p75^{NTR} DD

Comparison of the DD interfaces used for binding to RhoGDI and RIP2 CARD showed that these shared partially overlapping binding sites on p75^{NTR} DD (Figure 4A), indicating that RIP2 and RhoGDI cannot bind to the p75^{NTR} DD simultaneously due to steric hindrance. This is in agreement with our previous biochemical studies which identified overlapping epitopes required for the interaction of p75^{NTR} DD with both RIP2 and RhoGDI (Charalampopoulos et al., 2012). In order to better understand the hierarchical relationship of these interactions, we determined the binding affinities of the DD:RhoGDI and DD:CARD complexes by SPR. The Kd of RhoGDI binding to the p75^{NTR} DD was 0.82±0.3 μM, while the Kd of CARD binding to the DD was 4.67±0.7 nM (Figures 4B and C), indicating that RIP2 CARD binds with approximately 177-fold

higher affinity than RhoGDI to the $p75^{NTR}$ DD. This is in line with the larger buried solvent accessible area in the $p75^{NTR}$ DD:RIP2 CARD complex (~1400 $Å^2$) compared to that in the $p75^{NTR}$ DD:RhoGDI complex (~900 $Å^2$). Kinetic analyses revealed that CARD associates with the $p75^{NTR}$ DD with faster on-rate, and dissociates with slower off-rate, than RhoGDI (Table 3). The RIP2 CARD could still fold into a typical α-helical structure after deletion of the C-terminal tail (Figure 3—figure supplement 4A). However, the binding affinity of this construct to the $p75^{NTR}$ DD was 58.7±8.8 nM, i.e. approximately 12-fold lower than with the C-terminal tail (Figure 3—figure supplement 4B), indicating a significant contribution of the C-terminal tail to the association of RIP2 with $p75^{NTR}$.

The differential binding of RhoGDI and RIP2 CARD to the $p75^{NTR}$ DD was further tested through analysis of 2-D NMR spectra of RhoGDI binding to $p75^{NTR}$ DD in competition with RIP2 CARD. Figure 4D shows details of the RhoGDI spectra focusing on representative residues located in and/or close to the DD:RhoGDI interface. Addition of $p75^{NTR}$ DD produced a shift in the cross-peaks of these residues (red in Figure 4D), indicating binding of RhoGDI to the DD. Addition of RIP2 CARD to the RhoGDI:DD complex shifted these cross-peaks back to their initial positions (arrows in Figure 4D), indicating dissociation of RhoGDI from the $p75^{NTR}$ DD. These data demonstrate that RhoGDI and RIP2 CARD compete for binding to the $p75^{NTR}$ DD and that RIP2 CARD can displace RhoGDI from the receptor. In order to test the functional significance of the antagonism between RIP2 and RhoGDI, we assessed the levels of RhoA-GTP, a measure of RhoA activation, in cells transfected with a $p75^{NTR}$ expression construct in the absence or presence of increasing concentrations of a RIP2 construct (Figure 4E). While expression of $p75^{NTR}$ increased RhoA-GTP levels in transfected cells, co-expression of RIP2 decreased RhoA-GTP levels in a concentration dependent manner (Figure 4E), in agreement with an inhibitory role of RIP2 in $p75^{NTR}$-mediated activation of the RhoA pathway. In line with this, we found elevated levels of RhoA-GTP in brain extracts from *Rip2* knock-out mice compared to

wild type littermates (Figure 4F), suggesting that RIP2 can also restrict the activation of the RhoA pathway *in vivo*.

Solution structure of the p75^{NTR} DD homodimer

The current model of p75^{NTR} activation by neurotrophins predicts that the DDs should be in close proximity to each other to account for the high FRET state of the unliganded receptor. Purified rat p75^{NTR} DD has been shown to exist in either monomeric form or equilibrium between monomeric and dimeric forms depending on pH and counter ion (Vilar et al., 2014). However, the complete assignment of the DD homodimer was not reported in that study. We also found that human p75^{NTR} DD exists mainly in monomeric form in TRIS or HEPES buffer at pH 6.0-7.0, which were the buffer conditions used for structure determination of DD:RhoGDI and DD:CARD complexes. In phosphate buffer, however, we observed a new form of p75^{NTR} DD as revealed by the appearance of a new set of cross peaks in the [^{1}H-^{15}N] HSQC spectrum (Figure 5—figure supplement 1A and B). The set of cross peaks corresponding to monomeric DD was still visible, with nearly identical chemical shift but weaker intensity (Figure 5—figure supplement 1A), suggesting the co-existence of dimeric and monomeric DDs under these conditions. Dynamic lighter scattering (DLS) also indicated the formation of dimeric p75^{NTR} DDs in the presence of phosphate ions (Figure 5—figure supplement 1C and D). EGFP-tagged p75^{NTR} DDs showed anisotropic changes due to homodimerization at different DD concentrations. The apparent Kd of dimerization derived from anisotropic change was 49±15 μM (Figure 5—figure supplement 1E). This relatively low-affinity interaction may facilitate DD separation (low FRET state) upon receptor activation by neurotrophins.

In order to identify the dimerization interface, we determined the the NMR structure of the p75^{NTR} DD homodimer. The p75^{NTR} DD homodimer adopted a C2 symmetry (Figures 5A and 5B). A short C-terminal tail of 7 amino acids (Ser^{421}-Val^{427}) in each monomer remained disordered, similar to the DD:RhoGDI and DD:CARD complexes. The helical bundle, including the 3_{10} helix, did not undergo significant structural change

with an RMSD lower than 1.5Å compared to the other complexes. The dimerization interface consisted of α-helices H2 and H3 as well as residues in the H1-H2 and H3-H4 loops. Dimerization involved both charge and hydrophobic interactions. The key residues in the dimer interface included Asp^{357}, Arg^{360}, Thr^{377}, His^{378}, Glu^{379} and Ala^{380} (corresponding to Asp^{354}, Arg^{358}, Thr^{375}, His^{376}, Glu^{377} and Ala^{378} in rat $p75^{NTR}$ DD). This is in agreement with previous site-directed mutagenesis and NMR titration studies of the rat $p75^{NTR}$ DD homodimer (Vilar et al., 2014) (red labeled residues in Figure 5C). Cys^{381} (homologous to Cys^{379} in rat $p75^{NTR}$ DD) was also located in the dimerization interface but appeared in reduced form with a C^{β} chemical shift of 26.5 ppm. The distance between $Cys^{381}S^{\gamma}$ from each monomer was 6.7±0.1Å, i.e. too long for the formation of a disulphide bond. The buried solvent accessible area in the $p75^{NTR}$ DD homodimer was 573 $Å^2$, in line with the low affinity of the DD:DD interaction. We conclude that the two $p75^{NTR}$ DD protomers form a low-affinity, non-covalent homodimer in our structure.

The $p75^{NTR}$ DD homodimer interface defined in our NMR studies did not overlap with the RhoGDI binding site (Figures 6A and B). This is in agreement with the constitutive interaction of RhoGDI with the closed conformation of the receptor. On the other hand, the DD homodimer partially occluded the RIP2 CARD interaction surface (Figure 6C), indicating that interaction of RIP2 with $p75^{NTR}$ requires dissociation of the DD homodimer. We investigated whether the recruitment of RIP2 contributes to the separation of DDs triggered after neurotrophin binding to the receptor. This was done by taking real-time homo-FRET anisotropy measurements of DD:DD interaction in response to NGF in cells transfected with EGFP-tagged constructs of full length wild type $p75^{NTR}$ and a DD mutant deficient in RIP2 binding (Charalampopoulos et al., 2012) as previously described (Vilar et al., 2009). Application of NGF to cells expressing wild type $p75^{NTR}$ produced large oscillations of increased anisotropy at the cell membrane (Figure 6D), resulting in a positive net change averaged over 15 minutes treatment compared to vehicle (Figure 6E). As anisotropy is inversely related to FRET, this behavior indicates ligand-triggered separation of receptor intracellular

domains, as proposed earlier (Vilar et al., 2009). We note that the oscillations observed here are unlikely to represent the synchronous behavior of ensembles of receptors, as their average period (2-3 min) would seem too slow to reflect real molecular dynamics. Importantly, the $p75^{NTR}$ construct carrying mutations in the CARD binding site (CBS mutant) produced very similar anisotropy changes after NGF treatment (Figures 6D and 6E), indicating that recruitment of RIP2 is not required for DD separation in response to ligand binding to $p75^{NTR}$. Finally, we note that the DD homodimer interface also overlapped with several residues involved in neurotrophin-mediated activation of JNK, caspase-3 and the apoptosis pathway (Figure 6F) as identified in our previous studies (Charalampopoulos et al., 2012). Thus, while the structure and biochemical properties of the $p75^{NTR}$ DD homodimer support the ligand-independent interaction of RhoGDI with the receptor, they also demonstrate that dissociation of the $p75^{NTR}$ DD homodimer is required for recruitment of RIP2 and for activation of the JNK/caspase-3 pathway in response to neurotrophins.

Discussion

Novel heterotypic interactions in the death domain superfamily

The main paradigm in signal transduction by DD-containing proteins is oligomerization via homotypic DD interactions. Although $p75^{NTR}$ contains a DD which is required for downstream signaling, no intracellular $p75^{NTR}$ effectors containing canonical DDs have been identified. The study of DD signaling in $p75^{NTR}$ therefore addresses an unexplored dimension of the repertoire of interactions and activities in the DD superfamily. Homotypic interactions between DDs have been classified as type I, II and III according to the interfaces involved (Park, 2011; Park et al., 2007b; Weber and Vincenz, 2001). Despite what might have been expected of homotypic interactions, all known interactions in the DD superfamily are asymmetric, that is, the interaction is mediated by different interfaces in each of the two interacting domains (e.g. Ia and Ib

for type I). Remarkably, none of the binding surfaces in the p75^{NTR} DD (or in RIP2 CARD) identified in this study show a close match to any of the 6 conserved surfaces that characterize classical type I, II and III interactions in the DD superfamily. The p75^{NTR} DD surface that binds RhoGDI is formed by residues in helices H1 and H6. A previous study had proposed helix 5 as a binding site to RhoGDI based on serial deletion analysis of the p75^{NTR} DD (Yamashita and Tohyama, 2003). This conclusion is not supported by our solution structure of the DD:RhoGDI complex, in which H5 appears at the opposite side of the interface (Fig. 2B), nor by previous structure-function studies (Charalampopoulos et al., 2012). This discrepancy highlights some of the pitfalls in serial deletion studies that disregard the three-dimensional structures of proteins. The surface in the p75^{NTR} DD that interacts with the CARD of RIP2 includes residues in helices H2, H3 and H6 plus residues in the H5-H6 loop. On the other side of this interaction, residues in helix H1 as well as the H3-H4 and H5-H6 loops form the binding surface on the CARD of RIP2. To the best of our knowledge, this p75^{NTR} DD:RIP2 CARD complex represents the first structural characterization of an heterotypic interaction in the DD superfamily. Our solution structure of this complex also revealed an additional interaction between residues in the C-terminal half of helix H5 of the p75^{NTR} DD and the C-terminal tail of RIP2, which extends beyond the RIP2 CARD. This additional contact confers approximately 5-fold increased binding affinity between the two proteins. Finally, the interface that mediates the p75^{NTR} DD homodimer involves residues located in helix H3 as well as the H1-H2 and H3-H4 loops. This surface is similar, but not identical, to the type IIIb surface, like the one identified in the DD of PIDD for interaction with RAIDD (Park et al., 2007b). Unlike the classical type IIIb surface, however, the DD:DD interaction in p75^{NTR} makes extensive use of residues in the H3 helix, and the same surface in the two interacting DDs is used to form a symmetric dimer. Further studies will be required to determine whether the interactions identified here for the p75^{NTR} DD are exceptions or else represent new types of interactions that are yet to be identified in other DD-containing proteins.

A symmetric DD homodimer in p75^{NTR}

The solution structure of the p75^{NTR} DD homodimer shows it is a symmetric, non-covalent dimer held together by low-affinity interactions involving residues in helix H3 and the H1-H2 and H3-H4 loops. The p75^{NTR} DD dimer interface is in agreement with sites of interaction with downstream effectors identified by the structures reported here and in our previous site-directed mutagenesis studies (Figure 6). This p75^{NTR} DD dimer structure is also in accordance with a recent mutagenesis study that identified residues important for dimerization of rat p75^{NTR} DD (Vilar et al., 2014), many of which are also implicated in our structure. On the other hand, our results do not support two crystallographic structures reported for the rat p75^{NTR} DD homodimer that suggested this to be either a covalent symmetric dimer, held by a disulphide bond between Cys^{379} residues, or a non-covalent asymmetric dimer (Qu et al., 2013). None of the currently available evidence derived from structural, mutagenesis or functional studies appears to support those crystal structures. Nevertheless, we can not at present rule out the possibility that p75^{NTR} DDs may under certain circumstances form alternative oligomeric complexes through different interfaces. A recent study has suggested that p75^{NTR} can form trimers in transfected cells based on the apparent molecular weights of p75^{NTR} species in SDS/PAGE (Anastasia et al., 2015). Our NMR studies of the p75^{NTR} DD do not support such conclusion as we have not found any evidence for the existence of DD trimers in any of the conditions tested. Another recent study has used solution NMR spectroscopy to investigate the mobility of the transmembrane and intracellular domains of p75^{NTR} incorporated into lipid-protein nanodiscs (Mineev et al., 2015). These authors found a high level of flexibility in the juxtamembrane domain of p75^{NTR}, an observation that we also reported in our earlier NMR studies of this domain (Liepinsh, 1997), but they could not detect self-association of intracellular domains. However, it is unclear whether the lipid detergent used to form the lipid-protein nanodiscs interacted with the p75^{NTR} DD and prevented its dimerization. A few detergent molecules, too few to affect DD rotational correlation time, would be sufficient to hinder DD:DD interactions.

Competitive protein-protein interactions define the hierarchical activation of downstream pathways in p75^{NTR} signaling

The mechanism underlying ligand-induced dissociation of RhoGDI from p75^{NTR} has remained unclear. As neurotrophins induce the release of RhoGDI and the recruitment of RIP2, we have speculated that RIP2 may displace RhoGDI from binding sites in the p75^{NTR} DD (Charalampopoulos et al., 2012). Our solution structures of the p75^{NTR} DD in complex with RhoGDI and the RIP2 CARD lend experimental support to this notion by showing how steric clashes between the two effector proteins preclude their simultaneous binding to the p75^{NTR} DD. SPR experiments indicated that RIP2 CARD binds with over 100-fold higher affinity to the p75^{NTR} DD than RhoGDI, and 2D-NMR competition studies demonstrated that RIP2 CARD can in fact displace RhoGDI from the receptor. The functional significance of this relationship was evidenced by the ability of RIP2 to decrease p75^{NTR}-mediated RhoA activation in a dose-dependent manner. Furthermore, the enhanced activation of the RhoA pathway observed in brain extracts of *Rip2* knock-out mice suggests that RIP2 may also restrict activation of this pathway *in vivo*. These results demonstrate how a hierarchy of binding affinities dictates the differential interaction of downstream effectors with p75^{NTR} and ultimately controls the logic of p75^{NTR} signaling.

A model for the early stages of p75^{NTR} engagement with the RhoA and NF-kB pathways

p75^{NTR} has been postulated to function as a “displacement factor” that releases RhoA from RhoGDI leading to RhoA activation (Yamashita and Tohyama, 2003). This model has led to the idea that the p75^{NTR} DD and RhoA may compete for binding to RhoGDI. On the other hand, biochemical experiments have shown that RhoA can associate with p75^{NTR} through RhoGDI and the three proteins can be recovered together in co-immunoprecipitation assays (Yamashita et al., 1999; Yamashita and Tohyama, 2003), a result that would be incompatible with the displacement concept. Our structural studies show that the p75^{NTR} DD and RhoA bind on opposites sides of the RhoGDI

molecule, allowing the formation of a tripartite DD:RhoGDI:RhoA complex. Using a model of this complex and our solution structure of the $p75^{NTR}$ DD homodimer, we have constructed a model of the hexameric complex of these proteins (Video 1). This model retains the 2-fold symmetry of the DD homodimer, and accommodates all 6 components without any steric clashes. How can these interactions lead to RhoA activation? Our SPR experiments showed that association of RhoGDI with the $p75^{NTR}$ DD reduced its affinity for RhoA by 15-fold. Close comparison of RhoGDI structures in the complexes with either $p75^{NTR}$ DD or RhoA revealed local structural perturbations in RhoGDI (Figure 2—figure supplement 1), suggesting a potential allosteric mechanism underlying the release and activation of RhoA upon RhoGDI biding to the receptor. Based on the present studies, we propose a model for the early stages of $p75^{NTR}$ engagement with the RhoGDI/RhoA and RIP2/NF-kB pathways based on differential binding affinities and competitive protein-protein interactions (Figure 7). At the plasma membrane, the $p75^{NTR}$ forms a dimer held together by interactions between its DD and TM domains (Figure 7A). Recruitment of the RhoGDI:RhoA complex brings RhoA close to the plasma membrane (Figure 7B). RhoGDI binding to the $p75^{NTR}$ DD weakens its interaction with RhoA, a lipid-modified protein, allowing it to equilibrate with the plasma membrane where it can be activated by membrane-associated guanine nucleotide exchange factors (GEFs) (Garcia-Mata et al., 2011). RhoA may thus be in equilibrium between the cell membrane and the RhoGDI:$p75^{NTR}$ complex, and the action of GEFs and GTPase-activating proteins (GAPs) may further contribute to the dynamics of this exchange (Figure 7B). Upon dissociation from $p75^{NTR}$, e.g. as a consequence of RIP2 recruitment in response to NGF binding, RhoGDI regains high affinity for RhoA, extracting it from the membrane and holding it back in the cytosol in an inactive state (Figure 7C). This new view of the $p75^{NTR}$ DD in the activation of RhoA is in better agreement with the emerging role of RhoGDI as a general facilitator of small GTPase activity cycles. Recruitment of RIP2 to $p75^{NTR}$ ultimately leads to increased NF-kB activity by as yet unknown mechanisms. Another $p75^{NTR}$ interactor, TRAF6, is also a known regulator of the NF-kB pathway (Khursigara et al., 1999; Ye et al., 1999). As

TRAF6 has been shown to interact with the juxtamembrane region of $p75^{NTR}$, but not with the DD, RIP2 and TRAF6 may be able to bind simultaneously to the receptor and together contribute to enhance NF-kB activity in response to neurotrophins.

Conclusions

The structural studies of DD signaling in $p75^{NTR}$ presented here uncovered novel heterotypic interactions not previously seen in other DD-containing complexes. They represent new ways by which DDs regulate intracellular signaling. NMR, biochemical and functional studies defined competitive interactions between RhoGDI and RIP2 CARD and between RIP2 CARD and the $p75^{NTR}$ DD homodimer. These interactions give us unique insights into the molecular mechanisms underlying $p75^{NTR}$ activation and signaling, and reveal how overlapping interfaces and differential binding affinities cooperate to orchestrate the hierarchical activation of downstream pathways in non-catalytic receptors.

Methods

Sample preparation

The cDNAs of human p75NTR DD (330-427), RhoGDI (2-204), RhoA (2-190), and RIP2 CARD (434-539) were amplified from total human embryonic stem (ES) cell cDNA and subcloned into pET32-derived expression vectors between BamH I and Xho I restriction sites. Each recombinant protein contains 16 additional residues (MHHHHHHSSGLVPRGS) at the N-terminal, including one 6×His tag. Unlabelled proteins were expressed in E.coli strain SoluBL21 (DE3) in LB or M9 medium. Protein samples were purified using Ni-NTA affinity chromatography, FPLC gel filtration (Superdex 75) and/or ionic exchange (MonoQ or MonoS). Isotopic labeling was carried out by expressing the proteins in M9 minimal medium containing 15N-NH4Cl and/or 13C-labeled glucose as the sole source of nitrogen and carbon. Protein complexes

were prepared by mixing individual purified domains. Due to the weak binding affinities of DD:RhoGDI and DD homodimer complexes, as well as solubility problems of the DD:CARD complex in salt-containing buffers, gel filtration chromatography could not be used to purify these protein complexes. For the p75NTR DD:RhoGDI complex, two double-labeled samples were prepared in 10 mM D18-HEPES, 10 mM D10-DTT, 1 mM EDTA and 0.01% sodium azide at pH6.9: (1) 0.5 mM 13C,15N-labeled p75NTR DD mixed with 2 mM unlabeled RhoGDI; (2) 0.5 mM 13C, 15N-labeled RhoGDI mixed with 2 mM unlabelled p75NTR DD. For the p75NTR DD:RIP2 CARD complex, two double-labeled samples were made in water with 10 mM D10-DTT: (1) 0.5 mM 13C, 15N-labeled p75NTR DD mixed with 1 mM unlabelled RIP2 CARD; (2) 0.5 mM 13C, 15N-labeled RIP2 CARD mixed with 1 mM unlabelled p75NTR DD. For the RIP2 CARD on its own, 0.7 mM 13C, 15N-labeled RIP2 CARD was prepared in 50 mM D10-DTT in water. For the p75NTR DD homodimer, 1 mM 13C, 15N-labeled p75NTR DD was mixed with 1mM unlabelled p75NTR DD in 50 mM phosphate buffer, 10 mM D10-DTT, 1 mM EDTA and 0.01% sodium azide at pH6.9.

NMR spectroscopy and structure calculations

NMR experiments were performed on a Bruker 800 MHz NMR spectrometer with a cryogenic probe at 28 °C. All spectra were processed with NMRPipe (Delaglio et al., 1995) and analyzed with NMRView supported by a NOE assignment plugin (Johnson and Blevins, 1994). Resonance assignments of backbone, aliphatic and aromatic side chains were obtained using previously described methods (Lin et al., 2006; Xu et al., 2006). Intra-molecular NOE restraints were obtained from 4D time-shared ^{13}C, ^{15}N-edited NOESY spectra (Xu et al., 2007). Inter-molecular NOEs were identified from ^{13}C,^{15}N-filtered 3D experiments (Zwahlen et al., 1997). Ambiguous NOEs were assigned with iterated structure calculations by DYANA (Herrmann et al., 2002). Final structure calculation was started from 100 conformers. Energy minimization of the 10 conformers with the lowest final target function values was performed in AMBER force field (Case et al., 2002). The mean structure was obtained from the 10 energy-

minimized conformers for each domain. PROCHECK-NMR (Laskowski et al., 1996) was used to assess the quality of the structures. All the structural figures were made using MOLMOL (Koradi et al., 1996) or Chimera (Pettersen et al., 2004). The coordinates of $p75^{NTR}$ DD:RhoGDI, RIP2 CARD, $p75^{NTR}$ DD:RIP2 CARD and $p75^{NTR}$ DD homodimer have been deposited with the Protein Data Bank with PDB IDs 2n80, 2n7z, 2n83 and 2n97, respectively.

Model structure calculations, structure-based alignments and structural comparison

The structure of DD:RhoGDI:RhoA was modeled using HADDOCK 2.2 (Dominguez et al., 2003). The starting structures for the trimer were the DD monomeric structure from the lowest-energy structure of $p75^{NTR}$ DD:RhoGDI complex and the crystal structure of human RhoGDI:RhoA(GDP) (PDB ID: 1CC0). The starting structures used to build the hexameric model were the lowest-energy structure of the $p75^{NTR}$ DD homodimer and the crystal structure of human RhoGDI:RhoA(GDP). NOE data between $p75^{NTR}$ DD and RhoGDI were employed to create interaction restraints for both trimer and hexamer. Totally, 1,000 rigid-body docking solutions were first generated by energy minimization. The best 100 structures according to intermolecular energies were subjected to semi-flexible simulated annealing in torsion angle space followed by a final refinement in explicit water. Pairwise structure-based alignment and comparison were carried out using a sequential structure alignment program (SSAP) available at the SSAP server (http://www.cathdb.info/cgi-bin/cath/SsapServer.pl).

Dynamic lighter scattering (DLS) and circular dichroism (CD)

The apparent hydrodynamic radii of $p75^{NTR}$ DD domain in HEPES or phosphate buffer at pH7.0 were examined by DLS (DynaPro, Protein Solutions Inc.) at 22 °C. The data were analyzed using Dynamics 5.0 software. The CD spectra of all samples were recorded on a Jasco J-810 spectropolarimeter equipped with a thermal controller at 22°C.

Surface plasmon resonance (SPR) and anisotropy measurements of DD homodimerization

All sensorgrams were recorded on a BIAcore T200 at 22°C. For experiments with captured $p75^{NTR}$ DD (ligand), purified $p75^{NTR}$ DD-His was captured onto NTA sensor chips via Ni2+/NTA chelation. Protein samples of purified RIP2 CARD or RhoGDI (analytes) were sequentially diluted in running buffer (10mM HEPES, 50mM NaCL, 0.005% Surfactant P20, 0.02% protease-free BSA at pH7.0) and injected over the surfaces at different concentrations post capture. Regeneration of the NTA surface was performed using 350mM EDTA. For experiments involving immobilised RhoA, unprenylated RhoA:GDP:Mg2+ was immobilized via amine coupling onto CM5 sensor chips. Unreacted carboxymethyl sites were capped by ethanolamine. Protein samples of analytes were sequentially diluted in running buffer (10 mM HEPES, 50 mM NaCl, 0.005% Surfactant P20, pH 7.0) and injected over the surfaces at different concentrations. To measure the binding of RhoGDI to RhoA, 1 mM MgCl2 and 100 μM GDP were also included in the running buffer. Binding affinities were expressed as equilibrium dissociation constants (Kd) determined by steady-state (Figures 2C and 2D) or kinetic analyses (Figures 4B, 4C and 3—figure supplement 4B) using the BIAevaluation software. One binding site model was used for fitting of SPR data.

For anisotropy measurements of DD homodimerization, a cDNA encoding Enhanced Green Fluorescent Protein (EGFP) carrying the A206K mutation (to prevent its dimerization) was linked to the C-terminal of the human $p75^{NTR}$ cDNA via DNA ligation and the chimera protein ($p75^{NTR}$ DD-EGFP) was expressed in E.Coli BL21(DE3) and purified by FPLC. $p75^{NTR}$ DD-EGFP was sequentially diluted in 50mM phosphate buffer at pH 7.0. The anisotropy value was obtained from the measurements of fluorescence intensity in both parallel and perpendicular emission modes using a BioTek Cytation Imaging Reader at room temperature. Dimer dissociation constants were obtained by nonlinear fitting of anisotropy measurements to an equation describing a monomer–dimer equilibrium (Martin and Martin, 1996).

602 **Plasmids, antibodies and mice**

603 Full-length cDNAs encoding human $p75^{NTR}$, RhoGDI and RIP2 were amplified from
604 human embryonic stem (ES) cell cDNA and subcloned in the pCDNA3 vector
605 backbone (Invitrogen) for protein expression in mammalian cells. Mutations and
606 epitope tags were introduced using QuickChange Site-Directed Mutagenesis Kit
607 (Stratagene) and verified by DNA sequencing. Normal expression of all constructs was
608 verified by immunoblotting. The origin of antibodies was as follows: ANT-007 anti-
609 $p75^{NTR}$ (for immunoprecipitation) from Alomone Labs; ab52987 anti-$p75^{NTR}$ (for
610 immunoblotting) and anti-RhoGDI from Abcam; anti-Myc from Cell Signaling
611 Technologies; anti-RIP2 from Enzo Life Sciences; anti-β-actin and anti-βIII-tubulin from
612 Sigma-Aldrich. Rip2 knock-out mice were obtained from Koichi Kobayashi and Richard
613 Flavell (Kobayashi et al., 2002).

614 **Cell culture, cell transfection, immunoprecipitation, immunoblotting and RhoA**
615 **activation assay**

616 HEK293 and COS-7 cells were obtained from ATCC and cultured under standard
617 conditions in DMEM supplemented with 10% fetal calf serum, 100 units/ml penicillin,
618 100 mg/ml streptomycin and 2.5 mM glutamine. HEK293 cells were transfected with
619 the polythylenimine (PEI) method. Briefly, cells were plated in a 10 cm tissue culture
620 dish at a confluency of 3 x 10^6 cells/dish in normal growth media. Twenty-four hours
621 after plating, the media was changed to growth media containing 1% v/v FBS.
622 Transfection mix was prepared by mixing 1 µg of plasmid with 3 µg of PEI (1mg/ml) in
623 DMEM. The transfection mix was left to stand at room temperature followed by addition
624 dropwise into culture plates. 24 hours after transfection, the transfected cells were
625 returned to normal growth media. After a further 24 hours, cells were placed in sera-
626 free media for 16 hours prior to harvest and lysis in 50 mM Tris/HCl pH7.5, 1 mM
627 EDTA, 270 mM Sucrose, 1% (v/v) Triton X-100, 1 mM benzamidine, 1 mM PMSF,
628 0.1% (v/v) 2-mercaptoethanol and in the presence of phosSTOP (Roche) phosphatase
629 inhibitor cocktail mix as per manufacturer instructions. The cellular extracts were then

centrifuged at 4°C top speed on a benchtop centrifuge for 15 min. The supernatant was collected and filtered using a 0.2μM syringe filter. Protein concentration was determined by Bradford Assay. For anisotropy microscopy, COS-7 cells were transfected with Fugene6 (Promega) according to manufacturer's instructions. For immunoprecipitation, cell extracts (0.5 mg protein) was incubated for 16 h at 4°C on a rotating wheel with 0.5μg of anti-p75 antibody (ANT-007, Alomone) attached to Protein G–Sepharose (7.5μl packed beads). The beads were collected by brief centrifugation (2 min,780 x g, 4°C), washed three times with 0.5 ml of Wash Buffer (50 mM Tris/HCl pH 7.5, 1 % (v/v) Triton X-100, 0.05% (v/v) 2-mercaptoethanol and 0.2 M NaCl). After the last wash, pelleted beads were aspirated off wash buffer followed by addition of Laemmli sample buffer and analysis by SDS-PAGE and Western Blot. Immunoblots were developed using the ECL Western Blotting Kit (Thermo Scientific) and exposed to Kodak X-Omat AR films. Image analysis and quantification of band intensities were done with ImageJ software (NIH). For RhoA activation assays, mouse cerebella were dissected from postnatal day (P) 7 pups. RhoA activity was evaluated in total cerebellar extracts or in lysates of transfected HEK293 cells using the RhoA G-Lisa kit (Cytoskeleton) following the manufacturer's instructions. Equal amount of protein was used from each sample as determined by Bradford Assay.

Homo-FRET anisotropy microscopy

Anisotropy microscopy was done as previously described (Vilar et al., 2009) in transiently transfected COS-7 cells. Images were acquired 24 hr post-transfection, using a Nikon Eclipse Ti-E motorized inverted microscope (Nikon, Japan) equipped with a X-Cite LED illumination system. A linear dichroic polarizer (Meadowlark Optics) was placed in the illumination path of the microscope, and two identical polarizers were placed in an external filter wheel at orientations parallel and perpendicular to the polarization of the excitation light. The fluorescence was collected via a CFI Plan Apochromat Lambda 40x, 0.95 NA air objective, and parallel and polarized emission images were acquired sequentially on an Orca CCD camera (Hamamatsu Photonics,

Japan). Data acquisition was controlled by the Metamorph software (Molecular Devices, USA). NGF (from Alomone Labs) or vehicle was added 3 min after the start of the time lapse at a concentration of 100 ng/ml. Anisotropy values were extracted from image stacks of 30 images acquired in both parallel and perpendicular emission modes every 30 s for a time period of 15 min after NGF addition. For each construct, 12-15 ROIs were measured in 3 independent transfections performed in duplicate. Fluorescence intensity and anisotropy images were calculated as described by Squire et al. (Squire et al., 2004). Wild-type and CARD binding site (CBS) mutant cDNA constructs of rat p75NTR were tagged at the C terminus with a monomeric version of EGFP (Clontech) carrying the A206K mutation that disrupts EGFP dimerization. The CBS p75NTR mutant corresponded to the triple mutant D355A/H359A/E363A described in our previous study (Charalampopoulos et al., 2012).

Author contributions

Z.L. and C.F.I. conceived and designed the project. Z.L. prepared all protein samples, performed all structural studies, some of the binding studies, and prepared the original figures. J.Y.T. performed RhoA activation studies in transfected cells and SPR studies on NTA chips, E.T.H.G performed co-immunoprecipitation studies, C.K. performed RhoA activation studies in *Rip2* knock-out mice, K.B.L. performed FRET anisotropy studies, J.G. contributed with molecular cloning and technical assistance. C.F.I. and Z.L. wrote the paper and prepared the figures.

The authors declare no competing interests.

Acknowledgements

We thank Chian Ming Low and Yoke Ping Cheong for assistance with FPLC; Jingsong Fan for NMR data collection; Liming Yang for help with SPR measurements; Pin Li for

human ES cell cDNA; Koichi Kobayashi and Richard Flavell for *Rip2* knock-out mice; Peter Verveer, Georgia Xouri and Philippe Bastiaens for advice on homo-FRET anisotropy; Lilian Kisiswa for preliminary experiments of RhoGDI phosphorylation; and Ket Yin Goh for technical assistance. Support for this research was provided by grants from the National Medical Research Council of Singapore (CBRG13nov012), Ministry of Education of Singapore (MOE2014-T2-1-120), National University of Singapore (Start-Up and Strategic ODPRT Awards), European Research Council (339237-p75ntr), Swedish Research Council (K2012-63X-10908-19-5), Swedish Cancer Society (13-0676) and Knut and Alice Wallenberg Foundation (KAW 2012.0270).

References

Anastasia, A., Barker, P.A., Chao, M.V., and Hempstead, B.L. (2015). Detection of p75NTR Trimers: Implications for Receptor Stoichiometry and Activation. J Neurosci *35*, 11911–11920.

Carter, B.D., Kaltschmidt, C., Kaltschmidt, B., Offenhäuser, N., Böhm-Matthaei, R., Baeuerle, P.A., and Barde, Y.-A. (1996). Selective activation of NF-kappa B by nerve growth factor through the neurotrophin receptor p75. Science *272*, 542–545.

Case, D.A., Pearlman, D.A., Caldwell, J.W., Cheatham, T.E., III, Wang, W.S., Ross, C.L., Simmerling, T.A., Darden, T.A., Merz, K.M., Stanton, R.V., et al. (2002). AMBER 7 (University of California, San Francisco).

Charalampopoulos, I., Vicario, A., Pediaditakis, I., Gravanis, A., Simi, A., and Ibanez, C.F. (2012). Genetic dissection of neurotrophin signaling through the p75 neurotrophin receptor. Cell Rep *2*, 1563–1570.

Dechant, G., and Barde, Y.A. (2002). The neurotrophin receptor p75(NTR): novel functions and implications for diseases of the nervous system. Nat Neurosci *5*, 1131–1136.

Delaglio, F., Grzesiek, S., Vuister, G.W., Zhu, G., Pfeifer, J., and Bax, A. (1995). NMRPipe: a multidimensional spectral processing system based on UNIX pipes. J. Biomol. NMR *6*, 277–293.

Dominguez, C., Boelens, R., and Bonvin, A. (2003). HADDOCK: A protein-protein docking approach based on biochemical or biophysical information. *125*, 1731–1737.

Feinstein, E., Kimchi, A., Wallach, D., Boldin, M., and Varfolomeev, E. (1995). The death domain: a module shared by proteins with diverse cellular functions. Trends Biochem Sci *20*, 342–344.

Ferrao, R., and Wu, H. (2012). Helical assembly in the death domain (DD) superfamily. Curr Opin Struct Biol *22*, 241–247.

Friedman, W.J. (2000). Neurotrophins induce death of hippocampal neurons via the p75 receptor. J Neurosci *20*, 6340–6346.

Garcia-Mata, R., Boulter, E., and Burridge, K. (2011). The “invisible hand”: regulation of RHO GTPases by RHOGDIs. Nat Rev Mol Cell Biol *12*, 493–504.

Gehler, S., Gallo, G., Veien, E., and Letourneau, P.C. (2004). p75 neurotrophin receptor signaling regulates growth cone filopodial dynamics through modulating RhoA activity. J Neurosci *24*, 4363–4372.

Herrmann, T., Güntert, P., and Wüthrich, K. (2002). Protein NMR structure determination with automated NOE assignment using the new software CANDID and the torsion angle dynamics algorithm DYANA. J Mol Biol *319*, 209–227.

Holm, L., and Rosenström, P. (2010). Dali server: conservation mapping in 3D. Nucleic Acids Res *38*, W545–W549.

Ibanez, C.F., and Simi, A. (2012). p75 neurotrophin receptor signaling in nervous system injury and degeneration: paradox and opportunity. Trends Neurosci *35*, 431–440.

735 Johnson, B.A., and Blevins, R.A. (1994). NMR View: A computer program for the
736 visualization and analysis of NMR data. J. Biomol. NMR *4*, 603–614.

737 Khursigara, G., Bertin, J., Yano, H., Moffett, H., DiStefano, P.S., and Chao, M.V. (2001).
738 A prosurvival function for the p75 receptor death domain mediated via the caspase
739 recruitment domain receptor-interacting protein 2. J Neurosci *21*, 5854–5863.

740 Khursigara, G., Orlinick, J.R., and Chao, M.V. (1999). Association of the p75
741 neurotrophin receptor with TRAF6. J Biol Chem *274*, 2597–2600.

742 Knowles, J.K., Rajadas, J., Nguyen, T.-V.V., Yang, T., LeMieux, M.C., Griend, L.V.,
743 Ishikawa, C., Massa, S.M., Wyss-Coray, T., and Longo, F.M. (2009). The p75
744 Neurotrophin Receptor Promotes Amyloid-beta(1-42)-Induced Neuritic Dystrophy In
745 Vitro and In Vivo. J Neurosci *29*, 10627–10637.

746 Kobayashi, K., Inohara, N., Hernandez, L.D., Galán, J.E., Nunez, G., Janeway, C.A.,
747 Medzhitov, R., and Flavell, R.A. (2002). RICK/Rip2/CARDIAK mediates signalling for
748 receptors of the innate and adaptive immune systems. Nature *416*, 194–199.

749 Koradi, R., Billeter, M., and Wüthrich, K. (1996). MOLMOL: a program for display and
750 analysis of macromolecular structures. J Mol Graph *14*, 51–5–29–32.

751 Laskowski, R.A., Rullmannn, J.A., MacArthur, M.W., Kaptein, R., and Thornton, J.M.
752 (1996). AQUA and PROCHECK-NMR: programs for checking the quality of protein
753 structures solved by NMR. J. Biomol. NMR *8*, 477–486.

754 Liepinsh, E. (1997). NMR structure of the death domain of the p75 neurotrophin
755 receptor. Embo J *16*, 4999–5005.

756 Lin, Z., Lin, Z., Xu, Y., Xu, Y., Yang, S., Yang, S., Yang, D., and Yang, D. (2006).
757 Sequence-specific assignment of aromatic resonances of uniformly 13C,15N-labeled
758 proteins by using 13C- and 15N-edited NOESY spectra. Angew. Chem. Int. Ed. Engl.
759 *45*, 1960–1963.

760 Longenecker, K., Read, P., Derewenda, U., Dauter, Z., Liu, X., Garrard, S., Walker, L.,
761 Somlyo, A.V., Nakamoto, R.K., Somlyo, A.P., et al. (1999). How RhoGDI binds Rho.
762 Acta Crystallogr D Biol Crystallogr *55*, 1503–1515.

763 Martin, R.B., and Martin, R.B. (1996). Comparisons of Indefinite Self-Association
764 Models. Chem. Rev. *96*, 3043–3064.

765 Mayle, S., Boyle, J.P., Sekine, E., Zurek, B., Kufer, T.A., and Monie, T.P. (2014).
766 Engagement of Nucleotide-binding Oligomerization Domain-containing Protein 1
767 (NOD1) by Receptor-interacting Protein 2 (RIP2) Is Insufficient for Signal Transduction.
768 J Biol Chem *289*, 22900–22914.

769 Mineev, K.S., Goncharuk, S.A., Kuzmichev, P.K., Vilar, M., and Arseniev, A.S. (2015).
770 NMR Dynamics of Transmembrane and Intracellular Domains of p75NTR in Lipid-
771 Protein Nanodiscs. Biophysical Journal *109*, 772–782.

772 Park, H.H. (2011). Structural analyses of death domains and their interactions.
773 Apoptosis *16*, 209–220.

774 Park, H.H., Lo, Y.-C., Lin, S.-C., Wang, L., Yang, J.K., and Wu, H. (2007a). The death
775 domain superfamily in intracellular signaling of apoptosis and inflammation. Annu Rev
776 Immunol *25*, 561–586.

777 Park, H.H., Logette, E., Raunser, S., Cuenin, S., Walz, T., Tschopp, J., and Wu, H.
778 (2007b). Death domain assembly mechanism revealed by crystal structure of the
779 oligomeric PIDDosome core complex. Cell *128*, 533–546.

780 Park, K.J., Grosso, C.A., Aubert, I., Kaplan, D.R., and Miller, F.D. (2010). p75NTR-
781 dependent, myelin-mediated axonal degeneration regulates neural connectivity in the
782 adult brain. Nat Neurosci *13*, 559–566.

783 Perini, G., Della-Bianca, V., Politi, V., Valle, Della, G., Dal-Pra, I., Rossi, F., and Armato,
784 U. (2002). Role of p75 neurotrophin receptor in the neurotoxicity by beta-amyloid
785 peptides and synergistic effect of inflammatory cytokines. J Exp Med *195*, 907–918.

786 Pettersen, E.F., Goddard, T.D., Huang, C.C., Couch, G.S., Greenblatt, D.M., Meng,
787 E.C., and Ferrin, T.E. (2004). UCSF Chimera--a visualization system for exploratory
788 research and analysis. J Comput Chem *25*, 1605–1612.

789 Qu, Q., Chen, J., Wang, Y., Gui, W., Wang, L., Fan, Z., and Jiang, T. (2013). Structural
790 Characterization of the Self-Association of the Death Domain of p75(NTR). PLoS ONE
791 *8*, e57839.

792 Roux, P.P., and Barker, P.A. (2002). Neurotrophin signaling through the p75
793 neurotrophin receptor. Prog Neurobiol *67*, 203–233.

794 Tnimov, Z., Guo, Z., Gambin, Y., Nguyen, U.T.T., Wu, Y.-W., Abankwa, D., Stigter, A.,
795 Collins, B.M., Waldmann, H., Goody, R.S., et al. (2012). Quantitative analysis of
796 prenylated RhoA interaction with its chaperone, RhoGDI. J Biol Chem *287*, 26549–
797 26562.

798 Tuffereau, C., Bénéjean, J., Blondel, D., Kieffer, B., and Flamand, A. (1998). Low-
799 affinity nerve-growth factor receptor (P75NTR) can serve as a receptor for rabies virus.
800 Embo J *17*, 7250–7259.

801 Underwood, C.K., and Coulson, E.J. (2008). The p75 neurotrophin receptor. Int J
802 Biochem Cell Biol *40*, 1664–1668.

803 Vicario, A., Kisiswa, L., Tann, J.Y., Kelly, C.E., and Ibanez, C.F. (2015). Neuron-type-
804 specific signaling by the p75NTR death receptor is regulated by differential proteolytic
805 cleavage. J Cell Sci *128*, 1507–1517.

806 Vilar, M., Charalampopoulos, I., Kenchappa, R.S., Simi, A., Karaca, E., Reversi, A.,
807 Choi, S., Bothwell, M., Mingarro, I., Friedman, W.J., et al. (2009). Activation of the p75

808 neurotrophin receptor through conformational rearrangement of disulphide-linked
809 receptor dimers. Neuron *62*, 72–83.

810 Vilar, M., Sung, T.-C., Chen, Z., García-Carpio, I., Fernandez, E.M., Xu, J., Riek, R.,
811 and Lee, K.-F. (2014). Heterodimerization of p45-p75 Modulates p75 Signaling:
812 Structural Basis and Mechanism of Action. PLoS Biol *12*, e1001918.

813 Wang, K.C., Kim, J.A., Sivasankaran, R., Segal, R., and He, Z. (2002). P75 interacts
814 with the Nogo receptor as a co-receptor for Nogo, MAG and OMgp. Nature *420*, 74–
815 78.

816 Weber, C.H., and Vincenz, C. (2001). The death domain superfamily: a tale of two
817 interfaces? Trends Biochem Sci *26*, 475–481.

818 Wong, S.T., Henley, J.R., Kanning, K.C., Huang, K.-H., Bothwell, M., and Poo, M.-M.
819 (2002). A p75(NTR) and Nogo receptor complex mediates repulsive signaling by
820 myelin-associated glycoprotein. Nat Neurosci *5*, 1302–1308.

821 Xu, Y., Xu, Y., Long, D., Yang, D., and Yang, D. (2007). Rapid data collection for protein
822 structure determination by NMR spectroscopy. J. Am. Chem. Soc. *129*, 7722–7723.

823 Xu, Y., Xu, Y., Zheng, Y., Fan, J.-S., Yang, D., and Yang, D. (2006). A new strategy for
824 structure determination of large proteins in solution without deuteration. Nat Methods
825 *3*, 931–937.

826 Yamashita, T., Tucker, K.L., and Barde, Y.A. (1999). Neurotrophin binding to the p75
827 receptor modulates Rho activity and axonal outgrowth. Neuron *24*, 585–593.

828 Yamashita, T., and Tohyama, M. (2003). The p75 receptor acts as a displacement
829 factor that releases Rho from Rho-GDI. Nat Neurosci *6*, 461–467.

830 Ye, X., Mehlen, P., Rabizadeh, S., VanArsdale, T., Zhang, H., Shin, H., Wang, J.J., Leo,
831 E., Zapata, J., Hauser, C.A., et al. (1999). TRAF family proteins interact with the

common neurotrophin receptor and modulate apoptosis induction. J Biol Chem *274*, 30202–30208.

Yoon, S.O., Casaccia-Bonnefil, P., Carter, B.D., and Chao, M.V. (1998). Competitive signaling between TrkA and p75 nerve growth factor receptors determines cell survival. J Neurosci *18*, 3273–3281.

Zwahlen, C., Legault, P., Vincent, S., Greenblatt, J., Konrat, R., and Kay, L.E. (1997). Methods for measurement of intermolecular NOEs by multinuclear NMR spectroscopy: Application to a bacteriophage lambda N-peptide/boxB RNA complex. *119*, 6711–6721.

Figure legends

Figure 1. Solution structure of the complex between the p75^{NTR} DD and RhoGDI.

A) Superposition of backbone heavy atoms of the ten lowest-energy structures of the human p75^{NTR} DD:RhoGDI complex. N- and C-termini are indicated.

B) Ribbon drawing of the lowest-energy conformer. Light brown, p75^{NTR} DD; Cyan, RhoGDI. N- and C-termini, as well as DD helices H1 and H6 are indicated.

C) Details of binding interface in the complex viewed in the same orientations as panel B, respectively. Key residues at the binding interface are labelled and depicted as stick models. Red labels denote interface residues functionally validated in our earlier mutagenesis study (Charalampopoulos et al., 2012).

D) Co-immunoprecipitation of wild type (WT) and DD point mutants of human p75^{NTR} with Myc-tagged RhoGDI in transfected HEK 293 cells. Antibodies used for immunoprecipitation (IP) and Western blotting (WB) are indicated. WCE, whole cell lysate. The immunoblots shown are representative of three independent experiments.

E) Co-immunoprecipitation of wild type (WT) and point mutants of Myc-tagged human RhoGDI with p75^{NTR} in transfected HEK 293 cells. Antibodies used for immunoprecipitation (IP) and Western blotting (WB) are indicated. WCE, whole cell extract. The immunoblots shown are representative of three independent experiments.

Figure 1—figure supplement 1. NMR spectra of DD:RhoGDI complex in 20mM HEPES at 28°C and pH 6.9.

A) [1H-15N] HSQC spectra of ^{15}N-RhoGDI in the absence (black) and presence (red) of p75^{NTR} DD. The concentration of RhoGDI and p75^{NTR} DD was 0.5mM and 2mM, respectively.

867 B) Representative slices from the $^{13}C,^{15}N$-filtered 3D NOESY spectrum.

868 C) [^{1}H-^{15}N] HSQC spectra of ^{15}N-RhoGDI in complex with $p75^{NTR}$ DD in the absence
869 (black) and presence (red) of 250mM NaCl.

870

871 **Figure 1—figure supplement 2. The N-terminal domain of RhoGDI does not bind**
872 **to $p75^{NTR}$ DD.**

873 [^{1}H-^{15}N] HSQC spectra of $p75^{NTR}$ DD in the presence of RhoGDI (black) and RhoGDI
874 without N-terminal domain (RhoGDI ΔN, red) at 28 °C and pH 6.9. Molar ratio of DD to
875 RhoGDI or to RhoGDI ΔN was 1:4.

876

877 **Figure 2. Structural model of tripartite complex between $p75^{NTR}$ death domain,**
878 **RhoGDI and RhoA.**

879 A) Superposition of backbone traces of the ten lowest-energy structures of $p75^{NTR}$
880 DD:RhoGDI:RhoA tripartite complex. N- and C-termini are indicated.

881 B) Ribbon diagram of a representative structure of $p75^{NTR}$ DD:RhoGDI:RhoA
882 heterotrimer complex. Light brown, $p75^{NTR}$ DD; Cyan, RhoGDI; Blue, RhoA. Mg^{2+} and
883 GDP appear in ball-and-stick models. $p75^{NTR}$ DD helices H1, H5 and H6 as well as N-
884 and C-termini are indicated.

885 C) Binding of RhoGDI to immobilized RhoA:GDP:Mg^{2+} measured by surface plasmon
886 resonance (SPR). Binding affinity was determined by steady-state analysis. One
887 binding site model was used for fitting of SPR data. The sensorgram shown is
888 representative from three independent experiments.

889 D) Binding of RhoGDI complexed with $p75^{NTR}$ DD (molar ration 1:2) to immobilized
890 RhoA:GDP:Mg^{2+} measured by SPR. Binding affinity was determined by steady-state

analysis. One binding site model was used for fitting of SPR data. The sensorgram shown is representative from three independent experiments.

E) Sensorgram showing lack of interaction between $p75^{NTR}$ DD (tested at 125 to 500nM) and immobilized RhoA:GDP:Mg^{2+}. The sensorgram shown is representative from three independent experiments.

Figure 2—figure supplement 1. Local structural differences in RhoGDI after interaction with either $p75^{NTR}$ DD or RhoA:GDP.

Ribbon diagram of RhoGDI from the complex with $p75^{NTR}$ DD (light brown) is shown in cyan, and from the complex with RhoA (blue) in red (from Longenecker et al., 1999). Main structural differences in RhoGDI are indicated by the dotted line circle.

Figure 3. Solution structure of RIP2 CARD and its complex with $p75^{NTR}$ DD.

A) Superposition of backbone heavy atoms of the ten lowest-energy structures of human RIP2 CARD. N- and C-termini are indicated.

B) Ribbon drawing of the lowest-energy conformer of human RIP2 CARD. N- and C-termini, as well as selected residues in the C-terminal tail are indicated.

C) Superposition of backbone heavy atoms of the ten lowest-energy structures of the human $p75^{NTR}$ DD:RIP2 CARD complex. N- and C-termini are indicated.

D) Ribbon drawing of the lowest-energy $p75^{NTR}$ DD:RIP2 CARD conformer. Light brown, $p75^{NTR}$ DD; Green, RIP2 CARD. N- and C-termini, as well as DD helices H2, H3 and H5 are indicated.

E and F) Details of binding interface in the complex viewed in the same orientations as panel D, respectively. Key residues at the binding interface are labelled and depicted

as stick models. Red labels denote interface residues functionally validated in our earlier mutagenesis study (Charalampopoulos et al., 2012).

G) Co-immunoprecipitation of wild type (WT) and point mutants of Flag-tagged human RIP2 with $p75^{NTR}$ in transfected HEK 293 cells. In the overexpression conditions used for this experiment, interaction of RIP2 with $p75^{NTR}$ was constitutive in the absence of ligand. Antibodies used for immunoprecipitation (IP) and Western blotting (WB) are indicated. WCE, whole cell extract. The immunoblots shown are representative of three independent experiments.

Figure 3—figure supplement 1. Structure comparison of CARD domains using a sequential structure alignment program (http://v3-4.cathdb.info/).

A) Overlap of RIP2 CARD (red) and NOD1 CARD (grey, PDB ID: 2B1W).

B) Surface charge of RIP2 CARD without C-terminal tail. Positive charge surface is colored in blue, negative in red and non-charged in white.

C) Surface charge of NOD1 CARD.

D) Statistics of pairwise alignment of CARDs from RIP2 and NOD1.

Figure 3—figure supplement 2. NMR Spectra of DD:CARD complex.

A) [^{1}H-^{15}N] HSQC spectra of $p75^{NTR}$ DD in water in the absence (black) and presence (red) of RIP2 CARD.

B) Representative slices from the ^{13}C,^{15}N-filtered 3D NOESY spectra. Asterisk denotes ambiguous NOE peak.

Figure 3—figure supplement 3. Structural comparisons of p75^{NTR} DD and RIP2 CARD domains.

A) Structural comparison between p75^{NTR} DD from the DD:RhoGDI (red) and DD:CARD (green) complexes.

B) Structural comparison between monomeric RIP2 CARD (cyan) and RIP2 CARD from the DD:CARD complex (light brown).

Figure 3—figure supplement 4. The C-terminal tail of RIP2 CARD contributes to its interaction with the p75^{NTR} DD.

A) CD spectra of CARD (orange) and CARD ΔC mutant lacking the C-terminal tail (blue).

B) Sensorgram of binding kinetics of CARD ΔC binding to p75^{NTR} DD at pH7.0. One binding site model was used for fitting of SPR data.

Figure 4. Structural basis for competitive interaction between RIP2 and RhoGDI on the p75^{NTR} DD.

A) Surface representation of p75^{NTR} DD (light brown) with overlapped ribbon drawings of RhoGDI (cyan) and RIP2 CARD (green). The expanded view shows detail of the overlapping interfaces demonstrating steric clashes between residues in RhoGDI and CARD (highlighted as stick models).

B and C) Binding of RhoGDI (B) and RIP2 CARD (including C-terminal tail) (C) to captured His-tagged p75^{NTR} DD measured by SPR. Colored lines represent experimentally recorded values at different concentrations and black lines are fitting data. Binding affinities were determined by kinetics analysis using one binding site model was used for fitting of SPR data. The sensorgrams shown are representative from three independent experiments.

D) [^{1}H-^{15}N] HSQC spectra of ^{15}N-RhoGDI showing the ability of RIP2 to displace RhoGDI from the p75^{NTR} DD. The panels show details of different regions of the spectra for RhoGDI alone (green), RhoGDI in the presence of p75^{NTR} DD (red), and RhoGDI in the presence of both p75^{NTR} DD and RIP2 CARD (blue). Representative RhoGDI residues located in and/or close to the DD:RhoGDI interface are labelled. Arrows denote shifts in the spectra of labeled RhoGDI residues upon addition of p75^{NTR} DD and RIP2 CARD. All the spectra were recorded at pH 6.9 and 28 °C. The concentrations of RhoGDI, p75^{NTR} DD and RIP2 CARD were 0.05mM, 0.2mM and 0.2mM respectively.

E) Analysis of RhoA-GTP levels in lysates of HEK293 cells transfected with p75^{NTR} and RIP2 expression constructs, as indicated. Increasing concentrations of RIP2 construct is indicated. The histogram shows average RhoA-GTP levels (from triplicate measurements) normalized to p75^{NTR} alone. Protein expression levels were controlled by Western blotting (not shown). *, P<0.01 vs. p75^{NTR} alone (t-Test).

F) Analysis of RhoA-GTP levels in cerebellar extracts prepared from P7 *Rip2* knock-out mice and wild type littermates (WT). The histogram shows average RhoA-GTP levels in WT (N=3) and KO (N=4) animals normalized to WT levels. *, P<0.05 vs. WT (t-Test).

Figure 5. Solution structure of the p75^{NTR} DD homodimer.

A) Superposition of backbone heavy atoms of the ten lowest-energy structures of the human p75^{NTR} DD homodimer. N- and C-termini are indicated.

B) Ribbon drawing of the lowest-energy conformer viewed perpendicular (top) and parallel (bottom) to the 2-fold symmetry axis. DD monomers are colored in light brown and orange. N- and C-termini, as well as DD helices H1, H2, H3 and H4 are indicated.

C) Detail of binding interface in the DD homodimer. The top image shows the same view as that in panel B, bottom. Key residues at the binding interface are labelled and

989 depicted as stick models. Red labels denote interface residues functionally validated in
990 a previous mutagenesis study (Vilar et al., 2014).

991

992 **Figure 5—figure supplement 1. Homodimerization of p75^{NTR} DD.**

993 A) [^{1}H-^{15}N] HSQC spectra of p75^{NTR} DD in HEPES buffer (black) and phosphate buffer
994 (red) at pH6.9 and 28 oC.

995 B) Representative slices from the ^{13}C,^{15}N-filtered 3D NOESY spectrum.

996 C) Apparent hydrodynamic radius (Rh) distribution of DD from DLS measurement in
997 HEPES (top) and phosphate buffer (bottom), respectively. The protein concentrations
998 used are ~0.2 mM.

999 D) Average Rh of DD in HEPES and phosphate buffers. The theoretical Rh of DD
1000 monomer (~10 kDa) and homodimer (~20 kDa) are ~1.6nm and ~2.2nm, respectively.

1001 E) Determination of monomer-dimer Kd using anisotropy change resulting from FRET.
1002 p75^{NTR} DD tagged with EGFP(A206K) in its C-terminus was used in these
1003 experiments. N=3.

1004

1005 **Figure 6. Relationship between p75^{NTR} DD dimer interface and sites of**
1006 **interaction with downstream effectors.**

1007 A) Surface presentation of p75^{NTR} DD with homodimer interface colored in blue. N- and
1008 C-termini are indicated.

1009 B, C and F) Representation of RhoGDI binding site (yellow in B) RIP2 CARD binding
1010 site (green in C) and JNK/caspase-3 activation sites (from (Charalampopoulos et al.,
1011 2012)) (red in F) on the p75^{NTR} DD surface showing overlap of DD homodimer

interface (blue) with CARD binding and JNK/caspase-3 activation sites but not with RhoGDI binding site. N- and C-termini are indicated.

D) Representative experiment showing traces of average anisotropy change after addition of NGF or vehicle in cells expressing wild type $p75^{NTR}$ or a CARD binding site mutant (CBS mut) that is unable to bind RIP2 (Charalampopoulos et al., 2012). Addition of NGF, but not vehicle, induced positive anisotropy oscillations above baseline (horizontal axis at 0) in both wild type and mutant receptor constructs.

E) Net anisotropy change over 15 minutes after addition of NGF or vehicle in cells expression wild type $p75^{NTR}$ or the CARD binding site mutant (CBS mut). Results are expressed as average ± SD (N=3 experiments; n=15–17 cells examined per experiment). **, $p < 0.001$ versus vehicle.

Figure 7. Competitive protein-protein interactions orchestrate coupling of $p75^{NTR}$ to the RhoGDI/RhoA and RIP2/NF-kB pathways.

Schematic drawing of a model for the coupling of $p75^{NTR}$ to the RhoGDI/RhoA and RIP2/NF-kB pathways based on the structural and biochemical studies presented above.

A) The $p75^{NTR}$ dimer in the cell membrane is held by homotypic interactions of DDs (light brown) and TM domains (blue).

B) RhoGDI (cyan) brings RhoA (dark purple) in proximity to the plasma membrane through its interaction with the DD of $p75^{NTR}$. While the 2-fold symmetry axis of the DD:RhoGDI:RhoA hexametric complex is likely to be perpendicular to the plasma membrane, its relative orientation is hypothetical. RhoGDI binding to the $p75^{NTR}$ DD decreases its affinity for RhoA by 15-fold, and allows equilibration of RhoA with the plasma membrane, where it can be activated by GEFs.

C) Neurotrophin binding induces a conformational change in $p75^{NTR}$ resulting in the separation of its DDs (Vilar et al., 2009), exposing binding sites to downstream effectors that couple to the JNK/caspase-3 or NF-kB pathways, including RIP2. Recruitment of RIP2 to the $p75^{NTR}$ DD is mediated by the interaction of its CARD (green) with a binding surface that partially overlaps with that occupied by RhoGDI. As the binding affinity of the RIP2 CARD for the $p75^{NTR}$ DD is 100-fold higher than that of RhoGDI, the recruitment of RIP2 displaces RhoGDI from the receptor. Released from the DD, RhoGDI regains higher affinity for RhoA, extracting it from the membrane and holding it back in the cytosol.

Video 1. Model of the hexameric complex between $p75^{NTR}$, RhoGDI and RhoA(GDP).

Animation around the 2-fold symmetry axis of the hexameric $p75^{NTR}$ DD:RhoGDI:RhoA(GDP) complex. $p75^{NTR}$ DD appears in light brown, RhoGDI in cyan and RhoA in blue.

Table Legends

Table 1. NMR and refinement statistics for $p75^{NTR}$ DD complexes and RIP2 CARD

Table 2. Structural statistics for the 10 lowest-energy structures of $p75^{NTR}$ DD:RhoGDI:RhoA Trimer and Hexamer [a]

Table 3. Association and dissociation binding constants of p75NTR DD binding to RhoGDI and RIP2 CARD

1058

Table 1. NMR and refinement statistics for $p75^{NTR}$ DD complexes and RIP2 CARD

NMR distance & dihedral constraints	DD:RhoGDI	RIP2 CARD	DD:CARD	DD:DD
Distance constraints				
Total NOE	3525	2107	3760	3344
Intra-residue	809	436	798	728
Inter-residue				
Sequential (|i-j| = 1)	1054	656	1130	986
Medium-range (|i-j| ≤ 4)	665	589	1016	892
Long-range (|i-j ≥ 5)	945	426	771	706
Intermolecular NOE	52	-	45	32
Total dihedral angle restraints [a]	222	132	260	280
Structure Statistics				
Violations (mean and s.d.)				
Distance constraints (Å)	0.36±0.02	0.25±0.01	0.36±0.03	0.28±0.01
Dihedral angle constraints (º)	3.50±0.46	2.75±0.28	3.37±0.28	2.86±0.59
Max. dihedral angle violation (º)	4.16	3.25	3.77	4.28
Max. distance constraint violation (Å)	0.39	0.26	0.44	0.29
Ramachandran Plot (allowed region)	99.8%	99.5%	99.8%	99.9%
Average RMSD (Å) [b]				
Heavy atoms	0.91±0.12	0.83±0.06	0.99±0.08	0.77±0.06
Backbone atoms	0.55±0.13	0.36±0.05	0.66±0.09	0.43±0.02

[a] Dihedral angle constraints were generated by TALOS based on C_α and C_β chemical shifts.

[b] Average r.m.s. deviation (RMSD) to the mean structure was calculated among 10 refined structures. Superimposing residues for DD:RhoGDI, RIP2 CARD, DD:CARD and DD:DD are 334-421 of DD with 70-204 of RhoGDI, 436-523 of RIP2 CARD, 334-420 of DD with 435-534 of RIP2 CARD and 334-421 of DD respectively. The total AMBER energy for DD:RhoGDI, RIP2 CARD, DD:CARD, and DD:DD are -9884±41, -4437±32, -7706 ±32 and -7161±18 kcal/mol respectively.

1059

1060

1061

Table 2. Structural statistics for the 10 lowest-energy structures of p75^{NTR} DD:RhoGDI:RhoA Trimer and Hexamer [a]

	Trimer	Hexamer
Backbone RMSD (Å)		
from the mean, full complex	0.61± 0.25	0.59±0.20
From the mean, all interfaces	0.58±0.22	0.48±0.13
Total Energy (kcal/mol)	-20721±137	-37682±210
Ramachandran plot (%) [b]		
Residues in the most favored regions	82.2	84.7
Residues in additional allowed regions	14.1	12.5
Residues in generously allowed regions	1.9	1.9
Residues in disallowed regions	1.8	0.9

[a] Structural statistics for the 10 lowest-energy conformers were obtained from HADDOCK calculation using NOEs between DD and RhoGDI.
[b] Ramachandran analysis was carried out using PROCHECK-NMR.

1062

Table 3. Association and dissociation binding constants of p75^{NTR} DD binding to RhoGDI and RIP2 CARD

	ka ($\mu M^{-1} \cdot s^{-1}$)	kd ($s^{-1} \cdot 10^{-3}$)	Kd (nM)
DD:RhoGDI	0.06±0.01	50±9	827±338
DD:CARD	0.72±0.34	3.32±1.5	4.67±0.7

1063
1064

1065

Figure 1

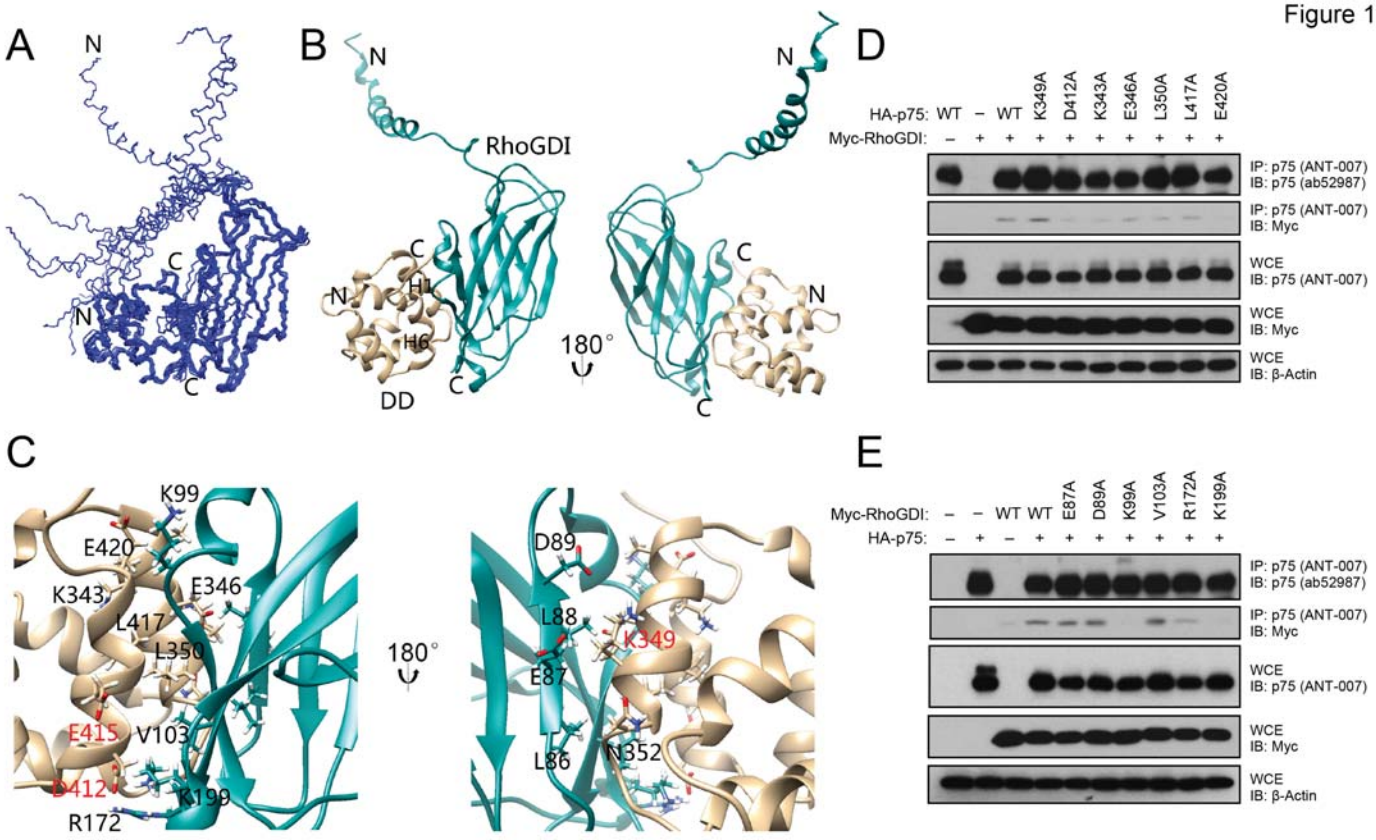
A
N
C
N
C
B
N
RhoGDI
C
N
H1
H6
DD
C
180°
N
C
N
C
D
HA-p75: WT – WT K349A D412A K343A E346A L350A L417A E420A
Myc-RhoGDI: – + + + + + + + + +
IP: p75 (ANT-007)
IB: p75 (ab52987)
IP: p75 (ANT-007)
IB: Myc
WCE
IB: p75 (ANT-007)
WCE
IB: Myc
WCE
IB: β-Actin
C
K99
E420
E346
K343
L417
L350
E415
V103
D412
K199
R172
180°
D89
L88
K349
E87
L86
N352
E
Myc-RhoGDI: – – WT WT E87A D89A K99A V103A R172A K199A
HA-p75: – + – + + + + + + +
IP: p75 (ANT-007)
IB: p75 (ab52987)
IP: p75 (ANT-007)
IB: Myc
WCE
IB: p75 (ANT-007)
WCE
IB: Myc
WCE
IB: β-Actin

Figure 2

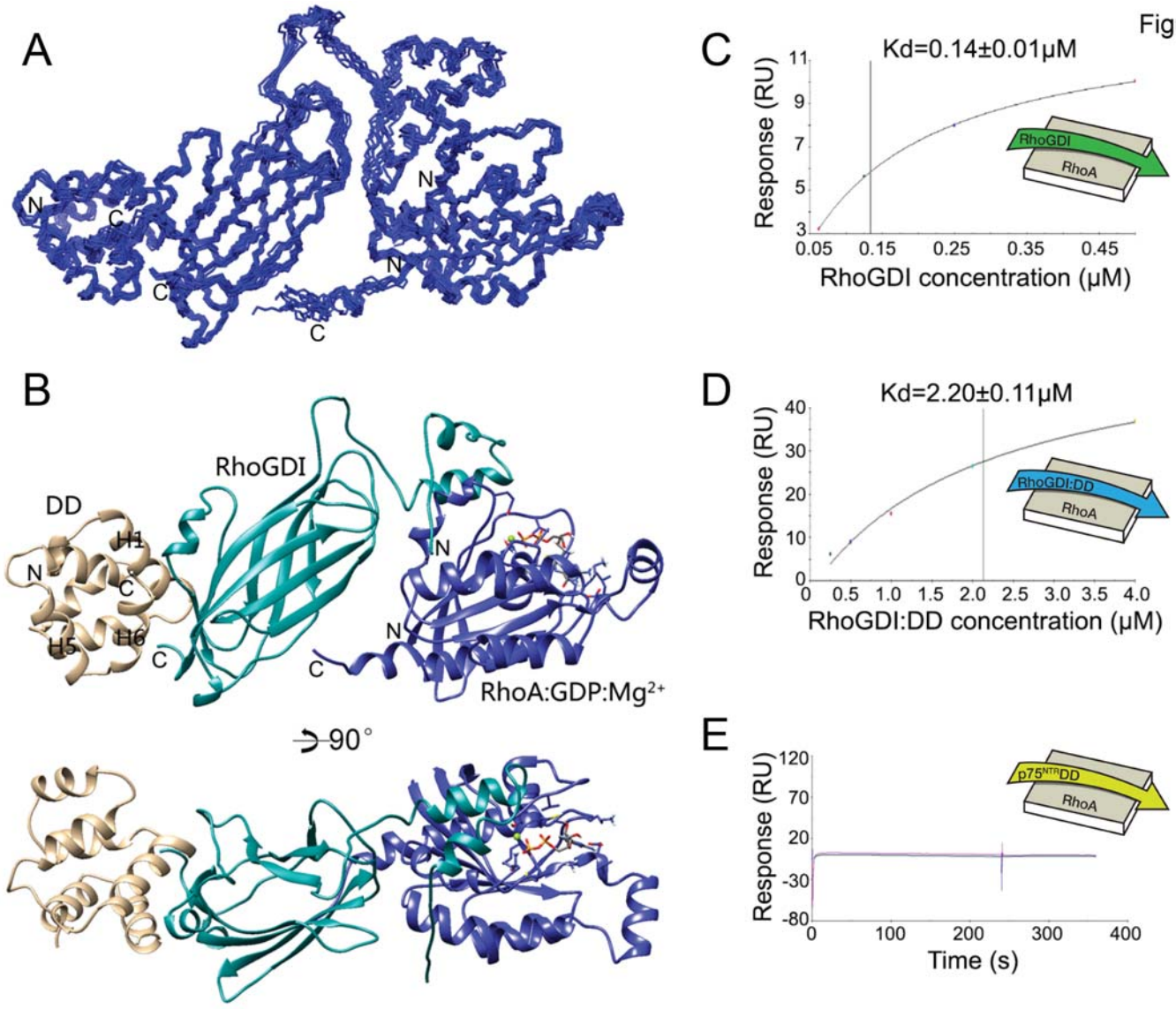
A
N
C
C
N
N
C
B
RhoGDI
DD
H1
N
C
H5
H6
C
N
N
C
RhoA:GDP:Mg2+
90°
C
Kd=0.14±0.01μM
Response (RU)
11
9
7
5
3
0.05
0.15
0.25
0.35
0.45
RhoGDI concentration (μM)
RhoGDI
RhoA
D
Kd=2.20±0.11μM
Response (RU)
40
30
20
10
0
0.5
1.0
1.5
2.0
2.5
3.0
3.5
4.0
RhoGDI:DD concentration (μM)
RhoGDI:DD
RhoA
E
Response (RU)
120
70
20
-30
-80
0
100
200
300
400
Time (s)
p75NTRDD
RhoA

Figure 3

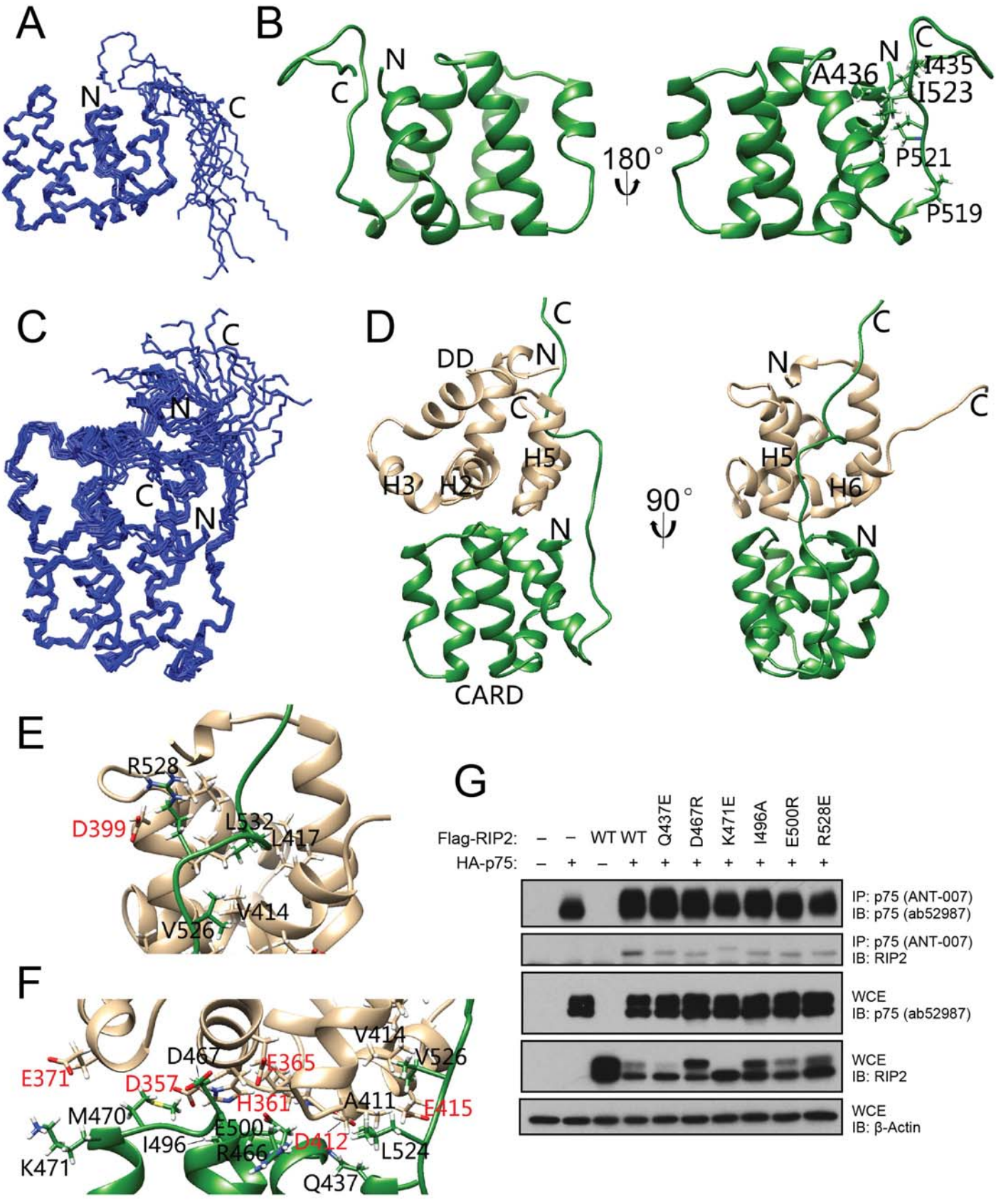
A
N
C
B
N
C
180°
N
C
A436
I435
I523
P521
P519
C
C
N
N
C
N
C
D
DD
N
C
H5
H3
H2
N
CARD
90°
C
N
C
H5
H6
N
E
R528
D399
L532
L417
V414
V526
F
V414
D467
E365
V526
E371
D357
H361
A411
E415
M470
E500
D412
I496
R466
L524
K471
Q437
G
Flag-RIP2: – – WT WT Q437E D467R K471E I496A E500R R528E
HA-p75: – + – + + + + + + +
IP: p75 (ANT-007)
IB: p75 (ab52987)
IP: p75 (ANT-007)
IB: RIP2
WCE
IB: p75 (ab52987)
WCE
IB: RIP2
WCE
IB: β-Actin

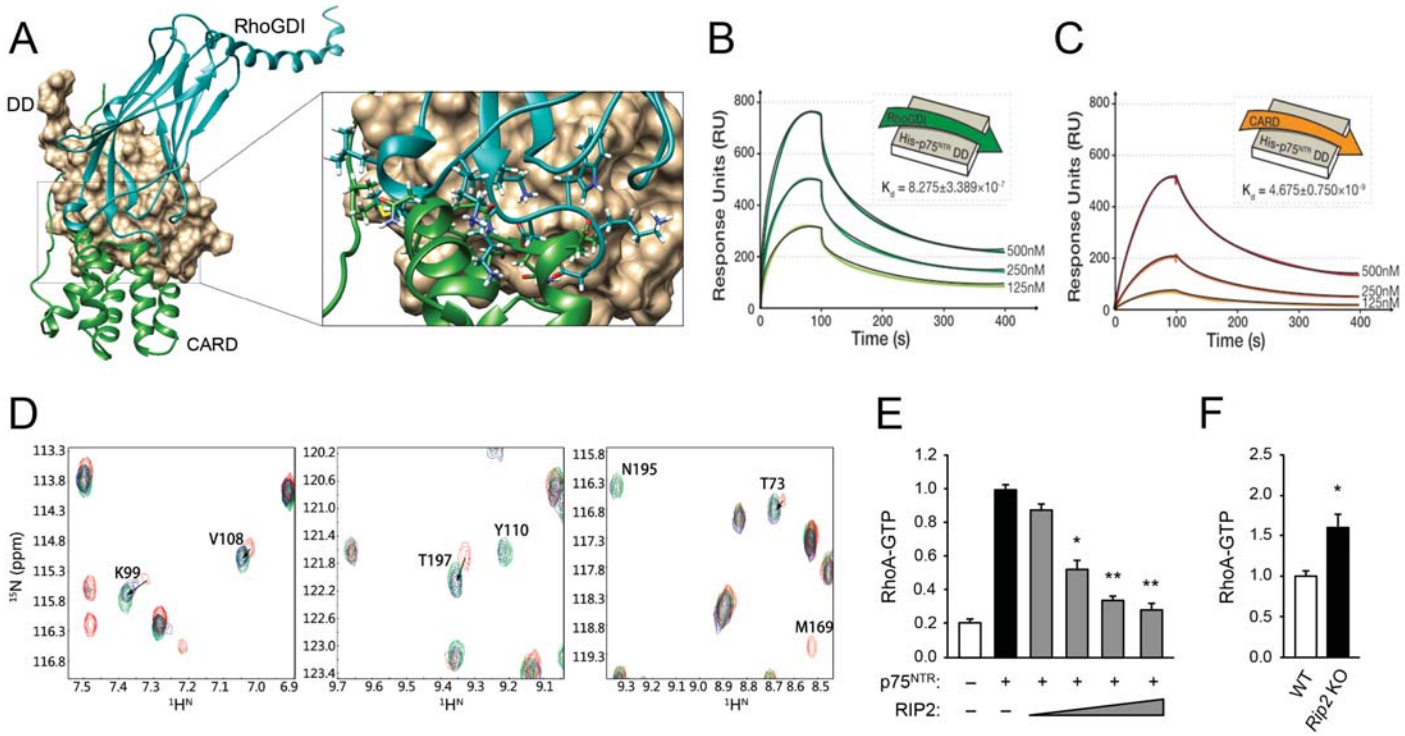
A
RhoGDI
DD
CARD
B
Response Units (RU)
Time (s)
RhoGDI
His-p75NTR DD
Kd = 8.275±3.389×10-7
500nM
250nM
125nM
C
Response Units (RU)
Time (s)
CARD
His-p75NTR DD
Kd = 4.675±0.750×10-8
500nM
250nM
125nM
D
15N (ppm)
1HN
K99
V108
T197
Y110
N195
T73
M169
E
RhoA-GTP
p75NTR:
RIP2:
F
RhoA-GTP
WT
Rip2 KO

Figure 5

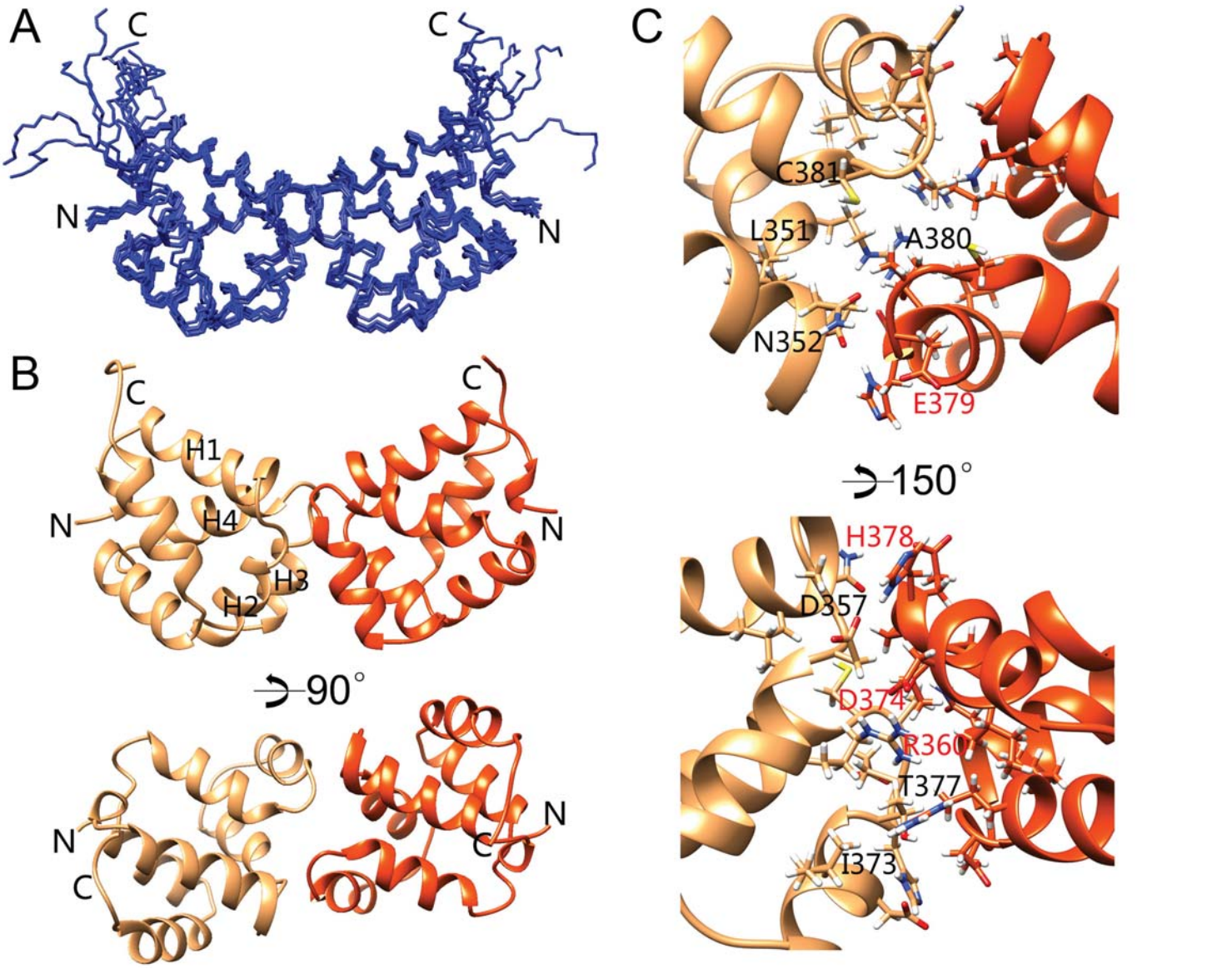
A
C
C
N
N
B
C
C
H1
N
H4
N
H3
H2
90°
N
C
C
N
C
150°
H378
D357
D374
R360
T377
I373
C381
L351
A380
N352
E379

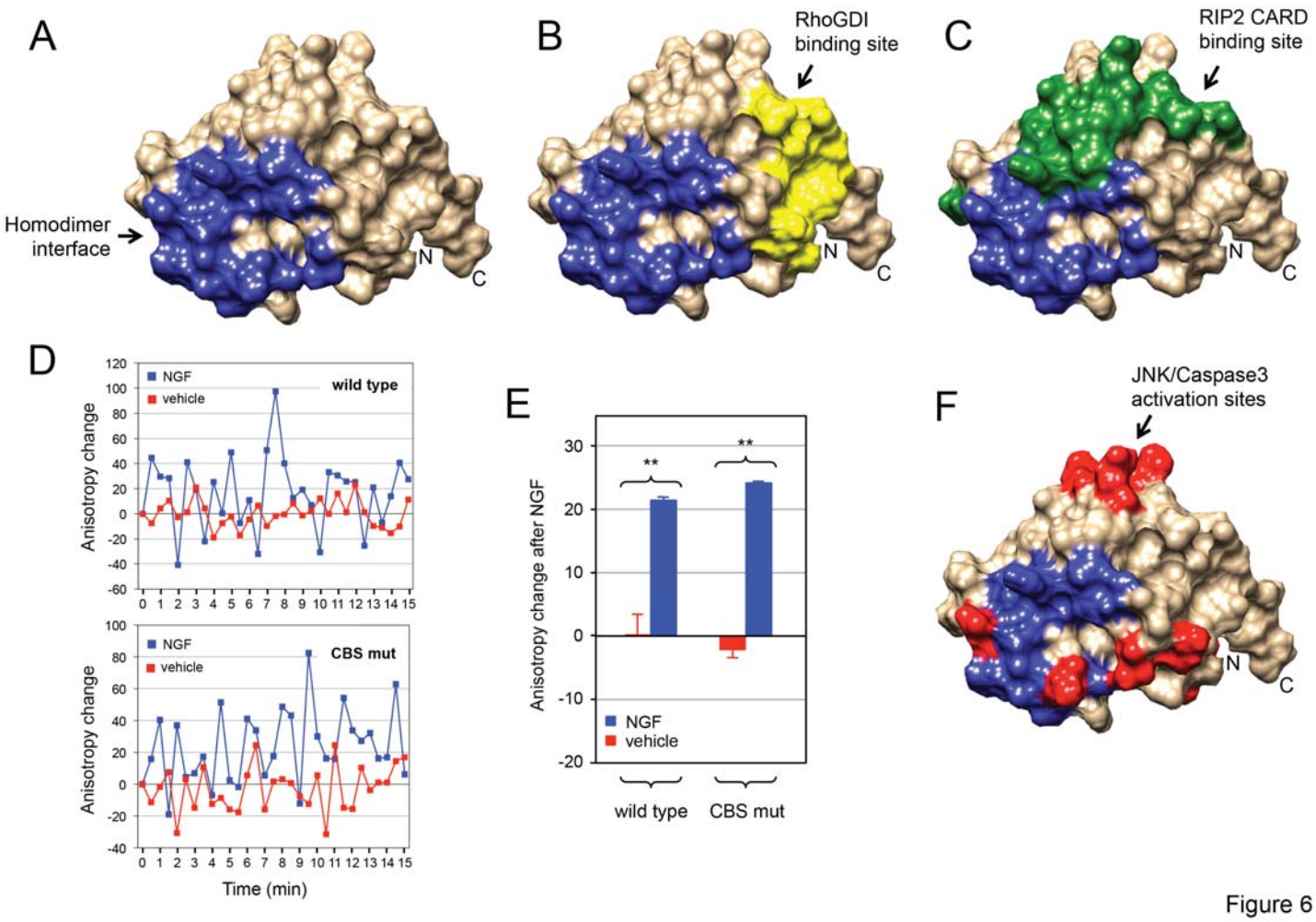
A
Homodimer interface
N
C
B
RhoGDI binding site
N
C
C
RIP2 CARD binding site
N
C
D
NGF
vehicle
wild type
Anisotropy change
CBS mut
Time (min)
E
Anisotropy change after NGF
**
**
NGF
vehicle
wild type
CBS mut
F
JNK/Caspase3 activation sites
N
C

Figure 6

Figure 7